Journal of

Applied and Computational Mechanics

Shahid Chamran
University of Ahvaz

Research Paper

On the Thermomechanical Behavior of Laminated Composite Plates using different Micromechanical-based Models for Coefficients of Thermal Expansion (CTE)

Noureddine Taibi[1] , Zakaria Belabed[2,3] , Belhadj Boucham[4] , Mohamed Benguediab[1] ,
Abdelouahed Tounsi[2,5,6,7] , Khaled Mohamed Khedher[8] , Mohamed Abdelaziz Salem[9]

[1] Laboratory of Materials and Reactive Systems, Department of Mechanical Engineering, Faculty of Technology, University of Sidi Bel Abbes, Algeria

[2] Material and Hydrology Laboratory, Civil Engineering Department, Faculty of Technology, University of Sidi Bel Abbes, Algeria

[3] Artificial Intelligence Laboratory for Mechanical and Civil Structures, and Soil, Institute of Technology, University Center of Naama, BP 66, 45000 Naama, Algeria

[4] Laboratory Mechanics of Structures and Solids (LMSS), Department of Mechanical Engineering, Faculty of Technology, University of Sidi Bel Abbes, Algeria

[5] Department of Civil and Environmental Engineering, King Fahd University of Petroleum & Minerals, 31261 Dhahran, Eastern Province, Saudi Arabia

[6] YFL (Yonsei Frontier Lab), Yonsei University, Seoul, Korea

[7] Lebanese American University, Beirut, Lebanon

[8] Department of Civil Engineering, College of Engineering, King Khalid University, Abha 61421, Saudi Arabia

[9] Department of Industrial Engineering, College of Engineering, King Khalid University, Abha 61421, Saudi Arabia

Abstract. In this paper, the influence of the Coefficient of Thermal Expansion (CTE) on the thermal stress analysis of laminated composite plates is explored. By introducing the undetermined integral terms in the displacement field, a new simple and efficient higher-order shear deformation theory is formulated for the thermo-mechanical behavior of thick laminated composite plates. This formulation aims to reduce the number of generated unknowns. Typically, a reduced order of the governing partial differential equations is expressed using the principle of virtual displacements. By using Navier's technique, closed-form solutions are derived for laminated composite plates under thermal and/or mechanical loading. Unfortunately, several traditional research investigations significantly depend on the rule of the mixture to determine reliable CTE for composites. This paper offers and examines a variety of analytical micromechanics-based models for estimating CTE in laminated composite materials, incorporating into consideration different considerations. The obtained results are compared to those given by other alternative plate theories, and the efficiency and accuracy of the present theory are demonstrated for the thermomechanical behavior of laminated composite plates. This study reviews and applies several micromechanics-based models, contrary to previous investigations. Laminated composite plates could delaminate or crack due to the matrix material's longitudinal CTE, affecting fiber volume fraction and stacking sequence. Micromechanics-based approaches are important when arbitrary thermo-mechanical characteristics can generate inaccuracies. Interestingly, micromechanics-based models can estimate effective CTE. Schapery, Chamberlain, and Chamis provide models with identical longitudinal CTE. For increasing fiber volume fractions, Chamberlain's model is more sensitive to increasing fiber volume fractions. Mechanical stress changes laminated plate behavior more than thermal loading. Although all presented micromechanical-based models have simplified representations, this research attempts to provide a standard for future investigations. The use of detailed micromechanical-based models stimulates further progress in understanding and utilizing complex composite plates.

Keywords: Thermomechanical analysis; laminated plates; advanced plate theory; coefficients of thermal expansion, micromechanical analysis.

1. Introduction

In recent years, advanced composites have received more interest in various engineering applications. Due to technological advancements, these materials are rapidly replacing alternatives in aeronautics, aerospace, and building sectors, as well as in the automotive industries. This development can be attributed to the exceptional mechanical and thermal properties of these composites, especially their density, which provides an important advantage. Consequently, realistic simulation of composites has evolved into a significant field for exploration. In several service environments, the composites are exposed to various loading cases,

particularly temperature variations produced by industrial devices and equipment [1-7]. Accurate comprehension of the thermo-mechanical behavior of laminated composites s is crucial to guarantee their reliability and optimal performance across different operating situations. Using random or arbitrary thermo-mechanical parameters to analyze these plates can result in potential oversights altering their actual behavior in practical problem settings. Hence, it is crucial to depend on known micromechanics-based models. The determination of a reliable CTE at the microscopic level is of crucial significance in understanding the thermo-mechanical stress behavior of laminates at the macroscopic scale. In this spirit, considerable research has been conducted, focusing specifically on the estimation of the effective CTE in composite laminates. Chan et al. [8] derived an explicit form of equivalent hygro-thermal expansion coefficients of the lumped layer in laminated composites. Fellah et al. [9] evaluated the effect of transverse cracks on the effective CTE in composite laminates using the Schapery micromechanics-based model. Karadeniz and Kumlutasc [10] proposed a micromechanical analysis of CTE in laminates using finite element simulation, the used model is compared with various analytical micromechanics-based models and existing experimental data. Özdemir et al. [11] presented a multi-scale analysis method for heat conduction in heterogeneous materials by employing a computational homogenization approach. Dong [12] proposed a new model for predicting transverse thermal coefficients, comparing the results with those from finite element simulations. Shabana and Noda [13] evaluated the effective thermo-mechanical properties of composites by using both homogenization and finite element methods. Sakata et al. [14] formulated a homogenized CTE for fiber-reinforced composites based on the equivalent inclusion method and the perturbation method. Igor [15] developed a new formulation of thermal expansion for composite materials by using the cross-property connection between thermal expansion and thermal conductivity. Nomura and Ball [16] developed a new micromechanical formulation to assess the thermal expansions of unidirectional laminate composites across varied temperature fields. Tsukrov et al. [17] predicted the overall thermo-elastic properties of unidirectional composites with cylindrical orthotropic constituents by introducing elastic solutions over various load cases. Nawab et al. [18] presented a numerical model for CTE in laminates, validating their approach through experimental analysis. Ran et al. [19] proposed a new micromechanics-based model for determining the CTE of unidirectional fiber-reinforced composites. Zamri et al. [20] conducted both experimental and numerical analyses to predict the CTE of unidirectional Pultruded composites, the authors compared the obtained results to those of other well- established micromechanics-based models. Dong et al. [21] investigated experimentally and numerically the thermal expansion behaviors of unidirectional composites based on periodic temperature and displacement boundary conditions. Cao et al. [22] reported an experimental study to derive the thermal properties of in situ-grown graphene-reinforced copper matrix laminated composites. Liang et al. [23] discussed the influence of various parameters on the CTE of composite multilayered flaky gun propellants based on experimental analysis. Wang [24] introduced a novel homogenization technique for predicting the effective mechanical and hygrothermal properties of unidirectional composites. Vignoli et al. [25] conducted a comparative study to estimate the effective micromechanical elastic properties of composite materials using experimental tests. Graciani et al. [26] used new experimental technology to derive the longitudinal and transverse CTE in curved composite laminates. Recently, Rao et al. [27] proposed a micromechanics-based model to predict the hygro-thermo-elastic properties of fiber-reinforced composites with a functionally graded interphase. Using the Representative Volume Element approach, Sun et al. [28] introduced a multiscale model to evaluate the thermal expansion of 3D composites, accounting for porosity and fiber volume fraction.

In addition, the prediction of the thermal stresses in laminates requires a comprehensive understanding of the CTE and thermal characteristics distribution between the constituents at the meso- or micro-scale. The benefits of mathematical modeling for laminated plates include a cost-effective and alternative approach to predicting their thermal responses, considering the underlying mechanics at the macro level across a variety of problems. Various theories exist in the literature regarding the thermo-mechanical behaviors of composite laminated plates, based on the classical laminated plate theory and shear deformation laminated plate theories. The classical laminated plate theory omits shear deformations and often underestimates the mechanical response for thick laminated plates. Recently, attention has focused on developing an efficient shear deformation laminated plate theory to address the limitations of classical laminated plate theory. The first-order laminated plate theory includes transverse shear deformations with appropriate shear correction factors for composite materials. Higher-order laminated plate theories have been introduced to eliminate the need for shear correction factors and to emphasize the significance of transverse shear deformation effects on the mechanical responses of laminated composite plates. Zenkour [29] developed a unified higher-order shear deformation theory to investigate the static response of laminated plates subjected to thermo-mechanical loads. Khandelwal et al. [30] suggested an efficient two-dimensional (2D) higher-order zig-zag theory to study the thermo-mechanical behavior of both composites and sandwich laminates under thermo-mechanical loading. Sayyad et al. [31] reformulated a refined plate theory for thermo-elastic analysis of laminated composite plates. Using a sinusoidal higher-order laminated plate theory, Ghugal and Kulkarni [32] presented a closed-form solution for symmetric cross-ply laminated plates under both linear and nonlinear thermo-mechanical loads. Qilin and Zhen [33] formulated a new finite element model based on Reddy's theory to investigate the thermal stresses in laminated composite plates. Naik and Sayyad [34] assessed a new computational model that includes both transverse shear and normal deformations to analyze the laminated and sandwich plates under linear thermal load. Zhen and Xiaohui [35] discussed the effect of transverse normal thermal strain on the thermo-mechanical behavior of multilayered plates using Reddy's higher-order shear deformation laminated plate model. Based on both higher-order zigzag plate theory and the inverse hyperbolic function, Garg et al. [36] developed seven unknown displacement field variables to analyze the hygro-thermomechanical response of laminated composite and sandwich plates. Joshan et al. [37] presented an analytical solution for studying the thermo-mechanical response of laminated composite plates using an inverse hyperbolic shear deformation theory. Joshan et al. [38] proposed a new non-polynomial shear deformation theory with only four variables to examine the effect of hygro-thermo-mechanical parameters on the static behavior of laminated composite plates. The formulated displacement field includes undetermined integral terms to reduce the number of generated unknowns and their related governing equations. Moradi and Mansouri [39] simulated laminated plates using the Differential Quadrature Method (DQM) to predict the critical temperature under uniform temperature distribution and arbitrary boundary conditions. Zenkour et al. [40] resolved the bending problem of laminated plates by considering various temperature distributions and elastic foundation parameters. Sing et al. [41] used a refined higher-order laminated plate theory in conjunction with the radial basis formulation to evaluate the critical buckling thermo-mechanical loads. Liu et al. [42] formulated a hexahedron hierarchical finite element based on 3D elastic theory and differential quadrature procedure to analyze the thermo-elastic behavior of laminated plates and shells. Han et al. [43] developed a new generalized higher-order zigzag theory to predict the thermo-mechanical behavior of laminated composite plates. Zhen and Chen [44] proposed a refined global/local higher-order laminated plate theory with finite element formulation to simulate the effect of hygro-thermo-mechanical loading on laminated plate responses. Zuo et al. [45] proposed a wavelet finite element model based on higher-order plate theory to study the coupling thermo-mechanical response of laminated composites. Upadhyay et al. [46] studied the nonlinear bending response of laminated composites under hygro-thermo-mechanical loads by using a higher-order shear deformation plate theory. Mechab et al. [47] presented a detailed investigation of the thermo-mechanical problem of laminated composite plates using a refined higher-order plate theory. Belbachir et al. [48] developed a new higher-order plate theory including undetermined integral terms to describe both normal and shear strains of laminated composite plates subjected to nonlinear thermo-mechanical loads. Joshan et al. [49] assessed

various higher-order shear deformation plate theories to investigate the thermo-mechanical behavior of laminated composites. Chattibi et al. [50] used a refined four-variable sinusoidal theory to estimate the bending response of laminated composites under various thermo-mechanical load cases. Ameri et al. [51] exploited the advantage of a new Quasi-3D shear deformation plate theory to demonstrate the effect of hygro-thermo-mechanical load parameters on the bending of laminated thick composites. Maji and Mahato [52] reviewed recent research in focus dealing with the development and applications of shear deformation plate theories for laminated composites. Overall, these studies illustrate a modest correlation between the micromechanical analysis and the global/local behavior of laminated plates in a thermal environment. Mahapatra et al. [53] gave practical importance to micromechanics-based models to predict the thermal response of laminated panels by applying Chamis's approach to evaluate the hygro-thermo-elastic constants. Recently, Saidane et al. [54] presented a significant application of micromechanics-based models to evaluate the CTE of flax/green epoxy composites. In this study, both Schapery's and Chamis's models are explored to derive the transverse and longitudinal coefficients of linear thermal expansion for laminated composites with various fiber contents and temperature variations.

The key objective of this research is to highlight the potential effects of CTE on the overall behavior of laminated plates. At the outset, an innovative Quasi-3D shear deformation theory is developed to investigate the thermomechanical response of laminated composite plates. By using undetermined integral terms to describe the displacement field, this novel theory offers fewer unknown variables than previous higher-order theories on laminated plates. This method serves to reduce the differential order of the generated governing equations while also allowing for the stretching effect. The following part of this research looks into the effect of CTE on the general effectiveness of laminated plates under thermo-mechanical loading. In conclusion, the difficulty of obtaining directly comparable experimental data prompted us to focus on a comprehensive theoretical investigation. This claims the current work provides a solid theoretical basis that will aid future empirical investigations.

2. Theoretical Formulation

2.1. Geometrical aspect

Assume a laminated composite plate with a constant thickness h, included from rectangular Cartesian coordinates (x, y, z), as shown in Fig. 1. The top and bottom surfaces of the plate are each $z = \pm h/2$, respectively; the plate is composed of k-orthotropic layers with stacking sequences related to the angle of fiber arrangement for global coordinates [55].

2.2. Homogenization models for CTE of laminated composites

Consider a unidirectional composite layer subjected to normal or shear stresses under mechanical and/or thermal loads. The effective material properties, including the longitudinal and transverse modulus, in-plane shear modulus, and coefficient of thermal expansion (CTE), are determined through the application of micromechanics-based approaches. These approaches establish the relationship between the properties of a unidirectional layer and the inherent attributes of its constituent fibers and matrix. The micromechanical-based models presented are well-acknowledged and commonly employed in this field of research. Although new models are being developed, most of them are based on complex numerical investigations and are verified by comparing them with known models, like the adopted ones. These models provide a systematic framework for investigating small-scale interactions, enabling precise predictions on a large scale, particularly for the sophisticated characteristics of laminated composite materials. In thermo-mechanical cases, the assumed CTE is derived from both thermal strains dealing with material expansion and externally applied loads by resolving related systems of equilibrium, constitutive, and strain-displacement equations. To avoid these difficulties, the relative micromechanics-based models are considered to derive the CTE, such as Van Fo Fy, Schapery, Schneider Chamberlain, and Chamis micromechanics-based models. A typical laminated composite is formed by an arrangement of a set of orthotropic composite layers. The material properties of each layer are evaluated by using the volume fraction of the components (Fibers and Matrix). In this study, the volume fraction can be stated in the form [56]:

$$V_f = 1 - V_m \tag{1}$$

2.2.1. Van Fo Fy model

Based on the exact elasticity solution of the stress analysis where the fibers are embedded in an isotropic matrix, Van Fo Fy [57] formulated both the longitudinal and transverse CTE as:

$$\alpha_1 = \alpha_m - (\alpha_m - \alpha_f)\frac{(1+\nu_m)E_fV_f - (1+\nu_f)(E_1 - E_mV_m)}{(1+\nu_m)E_fV_f} \tag{2a}$$

$$\alpha_2 = \alpha_m + (\alpha_m - \alpha_1)\nu_{12} - (\alpha_m - \alpha_f)(1+\nu_f)\frac{(\nu_m - \nu_{12})}{(\nu_m - \nu_f)} \tag{2b}$$

2.2.2. Schapery model

According to Schapery's assumptions [58], effective CTE is derived from the extreme principles of thermo-elasticity in two-phase composites. Both in-plan and transverse CTE can be stated in the form:
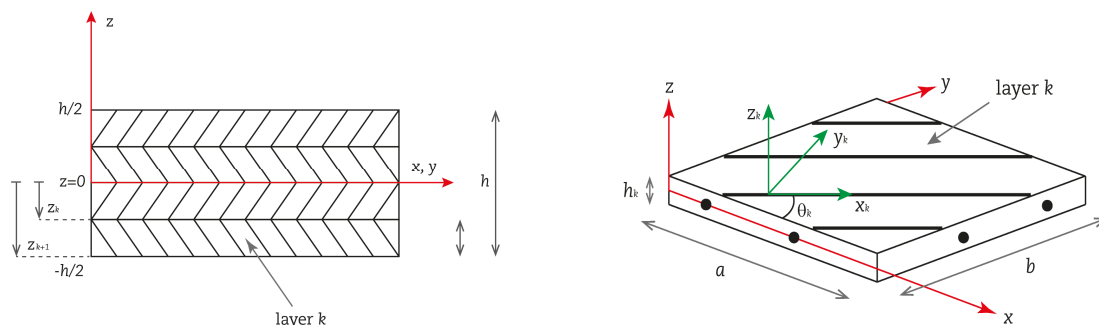

Fig. 1. Laminated composite plate with uniform thickness in the rectangular Cartesian coordinates: geometry and stacking sequence.

$$\alpha_1 = \frac{E_f V_f \alpha_f + E_m V_m \alpha_m}{E_f V_f + E_m V_m} \tag{3a}$$

$$\alpha_2 = (1 + \nu_f)\alpha_f V_f + (1 + \nu_m)\alpha_m V_m - \alpha_1(\nu_f V_f + \nu_m V_m) \tag{3b}$$

2.2.3. Schneider model

By taking into account the geometrical arrangement of fibers embedded in an elastic matrix, Schneider [59] formulated the transverse CTE of cylindrical fibers surrounded by a cylindrical matrix coat as:

$$\alpha_1 = \frac{E_f V_f \alpha_f + E_m V_m \alpha_m}{E_f V_f + E_m V_m} \tag{4a}$$

$$\alpha_2 = \alpha_m - (\alpha_m - \alpha_f)\left[\frac{2(1+\nu_m)(\nu_m^2 - 1)C}{\frac{1 + 1.1 V_f}{1.1 V_f - 1} - \nu_m + 2\nu_m^2 C} - \frac{\nu_m \frac{E_m}{E_f}}{\frac{1}{C} + \frac{E_m}{E_f}}\right] \tag{4b}$$

$$C = \frac{1.1 V_f}{1 - 1.1 V_f} \tag{4c}$$

2.2.4. Chamberlain model

Chamberlain proposed a novel micromechanics-based model based on the geometry of fiber packaging to predict the effective transverse CTE. This model is based on plane stress thick-walled cylinder equations for isotropic fibers embedded in an isotropic cylindrical matrix. The following sections explain the resultant effective transverse CTE derived from this model:

$$\alpha_1 = \frac{E_f V_f \alpha_f + E_m V_m \alpha_m}{E_f V_f + E_m V_m} \tag{5a}$$

$$\alpha_2 = \alpha_m + \frac{2(\alpha_f - \alpha_m)V_f}{\nu_m(F - 1 + V_m) + (F + V_f) + \frac{E_m}{E_f}(1 - \nu_f)(F - 1 + V_m)} \tag{5b}$$

2.2.5. Chamis model

Chamis's model is a widely used micromechanics-based model for the effective properties of laminated composite materials. It considers a basic force balance in a system of fiber loading that exhibits transverse isotropy. This approach is used to predict the homogenized properties of heterogeneous materials at the macroscopic scale, and the derived transverse thermal expansion expression is [60]:

$$\alpha_1 = \frac{E_f V_f \alpha_f + E_m V_m \alpha_m}{E_f V_f + E_m V_m} \tag{6a}$$

$$\alpha_2 = \alpha_f \sqrt{V_f} + \left(1 + \sqrt{V_f}\right)\left(1 + V_f \nu_m \frac{E_m}{E_f}\right)\alpha_m \tag{6b}$$

2.3. Elastic constants of laminated composites

Consider a unidirectional fiber-reinforced laminated composite; the effective mechanical properties are obtained using the micromechanics-based approach. Various simple micromechanics-based models are presented to derive the engineering elastic constants of laminated composites. In this study, three typical models are used: the Rule of Mixture (ROM), the Chamis model, and the Hill-Hashin-Christensen-Lo (HHCL) model [61, 62].

2.3.1. Rule of mixture

This model is widely used to generate the effective mechanical properties of composite materials. The fiber is considered embedded in a plate's matrix with a rectangular cross-section, and the same thickness is chosen for both the fiber and matrix of this composite for computational simplicity. By employing the principles of elasticity, the plane elastic moduli of the composite are derived by applying the different uniaxial load cases separately. The overall obtained elastic constants are given by:

$$\nu_{12} = V_f \nu_{12}^f + V_m \nu_m;$$
$$E_1 = V_f E_{11}^f + V_m E_m \ ; \ E_2 = \frac{E_m}{1 - V_f\left(1 - \frac{E_m}{E_{22}^f}\right)} \quad ;$$
$$G_{12} = \frac{G_m}{1 - V_f\left(1 - \frac{G_m}{G_{12}^f}\right)} \ ; G_{23} = \frac{G_m}{1 - V_f\left(1 - \frac{G_m}{G_{23}^f}\right)} \tag{7}$$

2.3.2. Chamis model

Since the rule of mixture overestimates the transverse and shear modulus compared to experimental tests, Hopkins and Chamis [63] developed a modified rule of mixture based on the packing geometry of the fiber and dividing the representative volume element into several subregions. By applying the stress state in each subregion and considering the fiber is embedded in an annular volume of the matrix, the six independent elastic properties are given as follows:

$$\nu_{12} = V_f \nu_{12}^f + V_m \nu_m; \tag{8}$$

$$E_1 = V_f E_{11}^f + V_m E_m; \ E_2 = E_3 = \frac{E_m}{1 - \sqrt{V_f}\left(1 - \frac{E_m}{E_{22}^f}\right)}$$

$$G_{12} = G_{13} = \frac{G_m}{1 - \sqrt{V_f}\left(1 - \frac{G_m}{G_{12}^f}\right)} \ ; \ G_{23} = \frac{G_m}{1 - \sqrt{V_f}\left(1 - \frac{G_m}{G_{23}^f}\right)}$$

2.3.3. Hill-Hashin-Christensen-Lo (HHCL) model

Based on Hill and Hashin's assumptions, the composite is made up of cylindrical fibers that are embedded in a cylindrical matrix. The upper and lower bounds for two-phase isotropic materials are defined by the variational energy principle of both strain and stress fields. The effective elastic constants are given as a function of bulk and shear modulus related to the fiber and matrix; the longitudinal and transverse Young modulus and longitudinal shear modulus can be stated in the form:

$$\nu_{12} = V_f \nu_{12}^f + V_m \nu_m + \frac{\left(\nu_{12}^f - \nu_m\right)^2 V_f(1 - V_f)}{\frac{V_f}{k_m} + \frac{1 - V_f}{k_f} + \frac{1}{G_{12}}}\left(\frac{1}{k_m} - \frac{1}{k_f}\right)$$

$$E_1 = V_f E_{11}^f + V_m E_m + \frac{4\left(\nu_{12}^f - \nu_m\right)^2 V_f(1 - V_f)}{\frac{V_f}{k_m} + \frac{1 - V_f}{k_f} + \frac{1}{G_{12}}}; \ E_2 = \frac{2}{\frac{0.5}{K_L} + \frac{0.5}{G_{23}} + \frac{2\nu_{12}^2}{E_1}}$$

$$G_{12} = G_m \frac{\left(G_{12}^f + G_m\right) + V_f\left(G_{12}^f - G_m\right)}{\left(G_{12}^f + G_m\right) - V_f\left(G_{12}^f - G_m\right)} \qquad (9)$$

$$k_f = \frac{E_{11}^f}{3\left(1 - 2\nu_{12}^f\right)} \ ; \ k_m = \frac{E_m}{3(1 - 2\nu_m)}$$

$$K_L = k_m + \frac{G_m}{3} + \frac{V_f}{\frac{1}{k_f - k_m + \frac{G_{12}^f - G_m}{3}} + \frac{1 - V_f}{k_m + \frac{4G_m}{3}}}$$

Christensen and Lo [62] provided further research to estimate the transverse shear modulus. Their approach is based on the lower bound of composites, demonstrating the differences in material properties or phases between fibers and matrix according to transverse shear loading. The resulting transverse shear modulus is represented by this equation:

$$G_{23} = G_m\left(1 + \frac{V_f}{\frac{G_m}{G_f - G_m} + \frac{\left(k_m + \frac{7G_m}{3}\right)}{\left(k_m + \frac{8G_m}{3}\right)}(1 - V_f)}\right) \qquad (10)$$

2.4. New Quasi-3D shear deformation laminated theory

The proposed shear deformation theory differs from other higher-order laminate theories in its ability to minimize the number of unknowns and governing equations, all without a requirement for shear correction factors. In addition, this theory incorporates the effect of stretching to overcome the limitations of 2D laminated plate theories. The importance of this stretching effect cannot be understated, especially in the context of thick laminated plates, and thus, it is crucial to consider this effect in our analyses.

2.4.1. Kinematics

According to [65-66], their suggested shear deformation plate theory relies on the following assumptions:
- The in-plane displacements follow the pattern established by the classical laminated plate theory, with additional integral terms that have yet to be determined,
- By applying a hyperbolic variation across the thickness coordinate to these undetermined integral terms, transverse shear strains and stresses are generated throughout the plate's thickness,
- Stress-free boundary conditions on the top and bottom surfaces of the plate can be established without the necessity of shear correction factors,
- The transverse displacement incorporates a stretching component in a manner that generates a hyperbolic variation across the thickness of the plate due to the normal stress to the plane.

Based on these assumptions, the corresponding displacement field is formulated and presented as follows:

$$u(x,y,z) = u_0(x,y) - z\frac{\partial w_0(x,y)}{\partial x} + k_1 f(z)\int \theta(x,y)dx \qquad (11a)$$

$$v(x,y,z) = v_0(x,y) - z\frac{\partial w_0(x,y)}{\partial y} + k_2 f(z)\int \theta(x,y)dy \qquad (11b)$$

$$w(x,y,z) = w_0(x,y) + g(z)\theta(x,y) \qquad (11c)$$

where the in-plane displacements u and v, and the transverse displacement w of a material point located at (x, y, z) in the plate. u_0, v_0, and w_0 represent the displacement unknowns at z = 0 (the mid-plane of a plate), the unknown $\int \theta(x,y)$ presents the undetermined integral term. The coefficients k_1 and k_2 depend on the geometry of the plate. Furthermore, the warping function $f(z)$ gives rise to the hyperbolic variation to vanish the shear stresses on the top and bottom surfaces of the laminated plate and is chosen as:

$$f(z) = \sinh\left(\frac{z}{h}\right)e^{\frac{1}{5h}\cosh\left(\frac{z}{h}\right)} + z\left[\frac{\cosh\left(\frac{1}{2}\right) + \frac{1}{5h}\sinh^2\left(\frac{1}{2}\right)}{-h}\right]e^{\frac{1}{5h}\cosh\left(\frac{1}{2}\right)} \qquad (12)$$

The related nonzero strains associated with the displacement field in Eqs. (11) are [53]:

$$\begin{Bmatrix} \varepsilon_x \\ \varepsilon_x \\ \gamma_{xy} \end{Bmatrix} = \begin{Bmatrix} \varepsilon_x^0 \\ \varepsilon_y^0 \\ \gamma_{xy}^0 \end{Bmatrix} + z \begin{Bmatrix} k_x^b \\ k_y^b \\ k_{xy}^b \end{Bmatrix} + f(z) \begin{Bmatrix} k_x^s \\ k_y^s \\ k_{xy}^s \end{Bmatrix} \tag{13a}$$

$$\begin{Bmatrix} \gamma_{yz} \\ \gamma_{xz} \end{Bmatrix} = g(z) \begin{Bmatrix} \gamma_{yz}^0 \\ \gamma_{xz}^0 \end{Bmatrix} \tag{13b}$$

$$\varepsilon_z = g'(z)\varepsilon_z^0 \tag{13c}$$

By substituting Eqs. (11) into Eqs. (13) the following strain– displacement relationships are obtained for the present Quasi-3D shear deformation laminated plate theory:

$$\begin{Bmatrix} \varepsilon_x^0 \\ \varepsilon_y^0 \\ \gamma_{xy}^0 \end{Bmatrix} = \begin{Bmatrix} \frac{\partial u_0}{\partial x} \\ \frac{\partial v_0}{\partial x} \\ \frac{\partial u_0}{\partial y} + \frac{\partial v_0}{\partial x} \end{Bmatrix} ; \begin{Bmatrix} k_x^b \\ k_y^b \\ k_{xy}^b \end{Bmatrix} = - \begin{Bmatrix} \frac{\partial^2 w_0}{\partial x^2} \\ \frac{\partial^2 w_0}{\partial y^2} \\ \frac{\partial^2 w_0}{\partial x \partial y} \end{Bmatrix} \tag{14a}$$

$$\begin{Bmatrix} k_x^s \\ k_y^s \\ k_{xy}^s \end{Bmatrix} = \begin{Bmatrix} k_1 \theta \\ k_2 \theta \\ k_1 \frac{\partial}{\partial y} \int \theta dx + k_2 \frac{\partial}{\partial x} \int \theta dy \end{Bmatrix} \tag{14b}$$

$$\varepsilon_z^0 = \theta \tag{14c}$$

where,

$$g(z) = \frac{df(z)}{28dz} \text{ and } g'(z) = \frac{dg(z)}{dz} \tag{15}$$

Based on Navier's method, the integral terms used in this formulation can be explicitly given as:

$$\frac{\partial}{\partial y} \int \theta dx = A' \frac{\partial^2 \theta}{\partial x \partial y} ; \frac{\partial}{\partial x} \int \theta dy = B' \frac{\partial^2 \theta}{\partial x \partial y},$$
$$\int \theta dx = A' \frac{\partial \theta}{\partial x} ; \int \theta dy = B' \frac{\partial \theta}{\partial y} \tag{16}$$

The coefficients A' and B' are relatively determined from Navier's method:

$$A' = -\frac{1}{\lambda^2} ; B' = -\frac{1}{\mu^2} ; k_1 = \lambda^2 ; k_2 = \mu^2 \tag{17}$$

where, $\lambda = m\pi/a$ and $\mu = n\pi/b$.

2.4.2. Constitutive relations

The linear constitutive relations of a laminated plate can be written as follows:

$$\begin{Bmatrix} \sigma_x \\ \sigma_y \\ \sigma_z \\ \tau_{yz} \\ \tau_{xz} \\ \tau_{xy} \end{Bmatrix}^{(k)} = \begin{bmatrix} \bar{Q}_{11} & \bar{Q}_{12} & \bar{Q}_{13} & 0 & 0 & 0 \\ & \bar{Q}_{22} & \bar{Q}_{23} & 0 & 0 & 0 \\ & & \bar{Q}_{33} & 0 & 0 & 0 \\ & & & \bar{Q}_{55} & 0 & 0 \\ & Sym & & & \bar{Q}_{44} & 0 \\ & & & & & \bar{Q}_{66} \end{bmatrix}^{(k)} \begin{Bmatrix} \varepsilon_x - \alpha_x \Delta T \\ \varepsilon_y - \alpha_y \Delta T \\ \varepsilon_z - \alpha_z \Delta T \\ \gamma_{yz} \\ \gamma_{xz} \\ \gamma_{xy} - \alpha_{xy} \Delta T \end{Bmatrix}^{(k)} \tag{18}$$

where $(\sigma_x, \sigma_y, \sigma_z, \tau_{yz}, \tau_{xz}, \tau_{xy})$ and $(\varepsilon_x, \varepsilon_y, \varepsilon_z, \gamma_{yz}, \gamma_{xz}, \gamma_{xy})$ are the stress and strain components of the kth layer, respectively, and $(\alpha_x, \alpha_y, \alpha_z, \alpha_{xy})$ are CTE. The temperature field is given in the generalized form:

$$T(x,y,z) = T_0(x,y) + \frac{z}{h} T_1(x,y) \tag{19}$$

where T_0 presents the constant temperature and T_1 is the linear distribution of the temperature.

The stiffness coefficients, $\bar{Q}_{ij}$ associated with each layer k of the laminated composite plate, can be expressed as:

$$\bar{Q}_{11} = Q_{11}c^4 + 2(Q_{12} + 2Q_{66})c^2s^2 + Q_{22}s^4;$$
$$\bar{Q}_{12} = (Q_{11} + Q_{22} - 4Q_{66})c^2s^2 + Q_{12}(s^4 + c^4);$$
$$\bar{Q}_{13} = Q_{13}c^2 + Q_{23}s^2;$$
$$\bar{Q}_{22} = Q_{11}s^4 + 2(Q_{12} + 2Q_{66})c^2s^2 + Q_{22}c^4;$$
$$\bar{Q}_{23} = Q_{13}s^2 + Q_{23}c^2;$$
$$\bar{Q}_{33} = Q_{33};$$
$$\bar{Q}_{44} = Q_{44}c^2 + Q_{55}s^2;$$
$$\bar{Q}_{55} = Q_{55}c^2 + Q_{44}s^2;$$
$$\bar{Q}_{66} = (Q_{11} + Q_{22} - 2Q_{12} - 2Q_{66})c^2s^2 + Q_{66}(s^4 + c^4);$$
$$\tag{20}$$

The elastic constants Q_{ij} are the three-dimensional elastic constants of orthotropic laminated, given by:

$$Q_{11} = \frac{1 - \nu_{23}\nu_{32}}{\Delta E_1 E_2} \; ; \; Q_{12} = \frac{\nu_{21} - \nu_{31}\nu_{23}}{\Delta E_2 E_3} = \frac{\nu_{12} - \nu_{32}\nu_{13}}{\Delta E_1 E_2}$$

$$Q_{13} = \frac{\nu_{31} + \nu_{21}\nu_{32}}{\Delta E_2 E_3} = \frac{\nu_{13} + \nu_{12}\nu_{23}}{\Delta E_1 E_2} \; ; \; Q_{22} = \frac{1 - \nu_{13}\nu_{31}}{\Delta E_1 E_3}$$

$$Q_{23} = \frac{\nu_{32} + \nu_{12}\nu_{31}}{\Delta E_1 E_3} = \frac{\nu_{23} + \nu_{21}\nu_{13}}{\Delta E_1 E_3} \; ; \; Q_{33} = \frac{1 - \nu_{12}\nu_{21}}{\Delta E_1 E_2} \quad (21)$$

$$Q_{44} = G_{23} \; ; \; Q_{55} = G_{13} \; ; \; Q_{66} = G_{12}$$

$$\Delta = \frac{1 - \nu_{12}\nu_{21} - \nu_{23}\nu_{32} - \nu_{31}\nu_{13} - 2\nu_{21}\nu_{32}\nu_{13}}{E_1 E_2 E_3}$$

2.4.3. Governing equations

Applying the principle of virtual work, reliable variational governing differential equations are derived to define the problem. This principle can be elaborated and expressed in the ways that follow:

$$0 = \int_A \left[\int_{-h/2}^{+h/2} (\delta U - \delta V) dz \right] dA \quad (22)$$

where δU is the variation in strain energy; and δV is the variation of potential energy. The variation of strain energy of the plate is given by:

$$\delta U = \int_A \left[\int_{-h/2}^{+h/2} (\sigma_x \delta\varepsilon_x + \sigma_y \delta\varepsilon_y + \sigma_z \delta\varepsilon_z + \tau_{yz}\delta\gamma_{yz} + \tau_{xz}\delta\gamma_{xz} + \tau_{xy}\delta\gamma_{xy}) \, dz \right] dA \quad (23)$$

$$= \int_A [N_x\delta\varepsilon_x^0 + N_y\delta\varepsilon_y^0 + N_{xy}\delta\gamma_{xy}^0 + N_z\delta\varepsilon_z^0 + M_x^b\delta k_x^b + M_y^b\delta k_y^b + M_{xy}^b\delta k_{xy}^b + M_x^s\delta k_x^s + M_y^s\delta k_y^s + M_{xy}^s\delta k_{xy}^s + S_{yz}^s\delta\gamma_{yz}^0 + S_{xz}^s\delta\gamma_{xz}^0]dA$$

where A is the top surface and the resultant forces and moments N, M, and S are defined as:

$$\begin{Bmatrix} N_x & N_y & N_{xy} \\ M_x^b & M_y^b & M_{xy}^b \\ M_x^s & M_y^s & M_{xy}^s \end{Bmatrix} = \int_{-h/2}^{+h/2} (\sigma_x ; \sigma_y ; \tau_{xy}) \begin{Bmatrix} 1 \\ z \\ f(z) \end{Bmatrix} dz \; ; \; N_z = \int_{-h/2}^{+h/2} \sigma_z g(z) dz \; ; \quad (24)$$

$$\begin{bmatrix} S_{yz}^s & Q_{yz}^s \\ S_{xz}^s & Q_{xz}^s \end{bmatrix} = \int_{-h/2}^{+h/2} \begin{Bmatrix} \tau_{yz} \\ \tau_{xz} \end{Bmatrix} \langle f'(z) \quad g(z) \rangle dz \; ;$$

The variation in the potential energy of the external applied loads can be expressed as:

$$\delta V = - \int_A q\delta w_0 dA \quad (25)$$

where q is the distributed mechanical transverse load.

Substituting Eqs. (23), and (25) into Eq. (22), taking the variations of δU and δV, integrating by parts, and setting each of the coefficients of δu_0, δv_0, δw_0 and $\delta\theta$, the following partial differential governing equations of the laminated plate are written as:

$$\delta u_0 : \frac{\partial N_x}{\partial x} + \frac{\partial N_{xy}}{\partial y} = 0 \quad (26a)$$

$$\delta v_0 : \frac{\partial N_{xy}}{\partial x} + \frac{\partial N_y}{\partial y} = 0 \quad (26b)$$

$$\delta w_0 : \frac{\partial^2 M_x^b}{\partial x^2} + 2\frac{\partial^2 M_{xy}^b}{\partial x \partial y} + \frac{\partial^2 M_y^b}{\partial y^2} = q \quad (26c)$$

$$\delta\theta : -k_1 A' M_x^s - k_2 B' M_y^s - (k_1 A' + k_2 B')\frac{\partial^2 M_{xy}^s}{\partial x \partial y} + k_1 A'\frac{\partial S_{xz}^s}{\partial x} + k_2 B'\frac{\partial S_{yz}^s}{\partial y} + \frac{\partial Q_{xz}^s}{\partial x} + \frac{\partial Q_{yz}^s}{\partial y} - N_z = 0 \quad (26d)$$

By substituting Eq. (24) into Eq. (18) and substituting the outcome results into Eq. (26), the resultant forces and moments are given as:

$$\begin{Bmatrix} N \\ M^b \\ M^s \end{Bmatrix} = \begin{bmatrix} A & B & B^s \\ B & D & D^s \\ B^s & D^s & H^s \end{bmatrix} \begin{Bmatrix} \varepsilon \\ k^b \\ k^s \end{Bmatrix} + \begin{bmatrix} L \\ L^\alpha \\ R \end{bmatrix} \varepsilon_z^0 \; ; S = A^s \gamma \quad (27)$$

$$N_z = R^\alpha \theta + L(\varepsilon_x^0 + \varepsilon_y^0) + L^\alpha(k_x^b + k_y^b) + R(k_x^s + k_y^s)$$

where,

$$N = \{N_x \quad N_y \quad N_{xy}\}; \; M^b = \{M_x^b \quad M_y^b \quad M_{xy}^b\}; M^s = \{M_x^s \quad M_y^s \quad M_{xy}^s\},$$

$$\varepsilon = \{\varepsilon_x^0 \quad \varepsilon_y^0 \quad \gamma_{xy}^0\}; \; k^b = \{k_x^b \quad k_y^b \quad k_{xy}^b\}; k^s = \{k_x^s \quad k_y^s \quad k_{xy}^s\} \quad (28)$$

and

$$A = \begin{bmatrix} A_{11} & A_{12} & 0 \\ A_{12} & A_{22} & 0 \\ 0 & 0 & A_{66} \end{bmatrix}; \ B = \begin{bmatrix} B_{11} & B_{12} & 0 \\ B_{12} & B_{22} & 0 \\ 0 & 0 & B_{66} \end{bmatrix}; \ D = \begin{bmatrix} D_{11} & D_{12} & 0 \\ D_{12} & D_{22} & 0 \\ 0 & 0 & D_{66} \end{bmatrix}; \tag{29a}$$

$$B^s = \begin{bmatrix} B_{11}^s & B_{12}^s & 0 \\ B_{12}^s & B_{22}^s & 0 \\ 0 & 0 & B_{66}^s \end{bmatrix}; \ D^s = \begin{bmatrix} D_{11}^s & D_{12}^s & 0 \\ D_{12}^s & D_{22}^s & 0 \\ 0 & 0 & D_{66}^s \end{bmatrix}; \ H^s = \begin{bmatrix} H_{11}^s & H_{12}^s & 0 \\ H_{12}^s & H_{22}^s & 0 \\ 0 & 0 & H_{66}^s \end{bmatrix} \tag{29b}$$

$$S = \{S_{xz}^s \quad S_{yz}^s\}, \ \gamma = \{\gamma_{xz} \quad \gamma_{yz}\}$$

$$A^s = \begin{bmatrix} A_{44}^s & 0 \\ 0 & A_{55}^s \end{bmatrix} \tag{29c}$$

$$\begin{Bmatrix} L_{i,j} \\ L_{i,j}^\alpha \\ R_{i,j} \end{Bmatrix} = \int_{-h/2}^{h/2} \bar{Q}_{ij} \begin{Bmatrix} [f'(z)]^2 \\ [g(z)]^2 \\ f'(z)g(z) \end{Bmatrix} dz \ (i = 1,2 \ and \ j = 3) \ ; R_{33}^\alpha = \int_{-h/2}^{h/2} \bar{Q}_{33}[g'(z)]^2 dz$$

Moreover, the stiffness components are given as:

$$\begin{Bmatrix} A_{11} & B_{11} & D_{11} \\ A_{12} & B_{12} & D_{12} \\ A_{66} & B_{66} & D_{66} \end{Bmatrix} = \int_{-h/2}^{h/2} \bar{Q}_{ij}(1 \quad z \quad z^2)dz \ ; \ \begin{Bmatrix} B_{11}^s & D_{11}^s & H_{11}^s \\ B_{12}^s & D_{12}^s & D_{12} \\ B_{66}^s & B_{66} & D_{66} \end{Bmatrix} = \int_{-h/2}^{h/2} \bar{Q}_{ij}(f(z) \quad zf(z) \quad f^2(z))dz \tag{30}$$

and

$$A_{44}^s = A_{55}^s = \int_{-h/2}^{h/2} \bar{Q}_{ij}[g(z)]^2 dz \tag{31}$$

Introducing Eq. (27) into Eq. (26), the equations of motion can be written in terms of displacements (u_0, v_0, w_0, θ), the related equations take the form:

$$A_{11}d_{11}u_0 + A_{66}d_{22}u_0 + (A_{12} + A_{66})d_{12}v_0 - B_{11}d_{111}w_0 - (B_{12} + 2B_{66})d_{122}w_0 + k_1 A' B_{11}^s d_{111}\theta$$
$$+ B_{66}^s(k_1 A' + k_2 B')d_{122}\theta + k_2 B' B_{12}^s d_{122}\theta + L_{13}d_1\theta = d_1 N_{xx}^T + d_2 N_{xy}^T; \tag{32a}$$

$$A_{22}d_{22}v_0 + A_{66}d_{11}v_0 + (A_{12} + A_{66})d_{12}u_0 - B_{22}d_{222}w_0 - (B_{12} + 2B_{66})d_{112}w_0 + k_1 A' B_{12}^s d_{112}\theta$$
$$+ B_{66}^s(k_1 A' + k_2 B')d_{112}\theta + k_2 B' B_{22}^s d_{222}\theta + L_{23}d_2\theta = d_2 N_{yy}^T + d_1 N_{xy}^T; \tag{32b}$$

$$B_{12}d_{111}u_0 + (B_{12} + 2B_{66})(d_{122}u_0 + d_{112}v_0) + B_{22}d_{222}v_0 - D_{11}d_{1111}w_0 - 2(D_{12} + 2D_{66})d_{1122}w_0 - D_{22}d_{2222}w_0 + k_1 A' D_{11}^s d_{1111}\theta$$
$$+ k_2 B' D_{22}^s d_{2222}\theta + (D_{12}^s + 2D_{66}^s)(k_1 A' + k_2 B')d_{1122}\theta + L_{13}^\alpha d_{11} + L_{23}^\alpha d_{22}\theta = q + d_{11}M_{xx}^T + d_{22}M_{yy}^T + d_{12}M_{xy}^T; \tag{32c}$$

$$-(B_{11}^s k_1 + B_{12}^s k_2 - L_{13})d_1 u_0 - B_{66}^s(k_1 A' + k_2 B')(d_{122}u_0 + d_{112}v_0) - (B_{12}^s k_1 + B_{22}^s k_2 - L_{23})d_2 v_0 + (D_{11}^s k_1 + D_{12}^s k_2 + L_{13}^\alpha)d_{11}w_0$$
$$+ 2D_{66}^s(k_1 A' + k_2 B')d_{1122}w_0 + (D_{12}^s k_1 + D_{22}^s k_2 + L_{23}^\alpha)d_{22}w_0 - (R_{13}k_1 + R_{23}k_2 + R_{33}^\alpha)\theta$$
$$- (H_{11}^s A' k_1^2 + H_{12}^s A' k_1 k_2 + R_{13}A' k_1 + (A' k_1)^2 + A_{55}^s)d_{11}\theta - H_{66}^s(k_1 A' + k_2 B')^2 d_{1122}\theta$$
$$- (H_{22}^s B' k_2^2 + H_{12}^s B' k_1 k_2 + R_{23}B' k_2 + (B' k_2)^2 + A_{44}^s)d_{22}\theta = -(k_1 P_{xx}^T + k_2 P_{yy}^T) - (k_1 A' + k_2 B')d_{12}P_{xy}^T - N_z^T \tag{32d}$$

where d_i, d_{ij}, d_{ijl}, d_{ijlk} are the following differential operators:

$$d_i = \frac{\partial}{\partial x_i}, d_{ij} = \frac{\partial^2}{\partial x_i \partial x_j}, \ d_{ijl} = \frac{\partial^3}{\partial x_i \partial x_j \partial x_l}, \ d_{ijlk} = \frac{\partial^4}{\partial x_i \partial x_j \partial x_l \partial x_k} \tag{33}$$

$$(i, j, l, k = 1,2) \ \text{and} \ (x_1 = x, x_2 = y)$$

The resultant forces and moments, due to thermal loading N^T, M^T and P^T are given as:

$$N^T = \{N_x^T \quad N_y^T \quad N_{xy}^T\}; \ M^T = \{M_x^T \quad M_y^T \quad M_{xy}^T\}; P^T = \{P_x^T \quad P_y^T \quad P_{xy}^T\} \tag{34}$$

and

$$\begin{Bmatrix} N_x^T & M_x^T & P_x^T \\ N_y^T & M_y^T & P_y^T \\ N_{xy}^T & M_{xy}^T & P_{xy}^T \end{Bmatrix} = \int_{-h/2}^{+h/2} \bar{Q}_{66} \begin{Bmatrix} \alpha_x \\ \alpha_y \\ \alpha_z \end{Bmatrix} (1 \quad z \quad f(z) \quad g'(z))T dz \ ; \tag{35}$$

3. Mathematical Resolutions

Examine a simply supported laminated composite plate with dimensions a and b. By applying Navier's solution procedure for the static problem, the following terms of displacements (u_0, v_0, w_0, θ) are assumed:

$$\begin{Bmatrix} u_0 \\ v_0 \\ w_0 \\ \theta \end{Bmatrix} = \sum_{m=1}^\infty \sum_{n=1}^\infty \begin{Bmatrix} U_{mn} \cos(\lambda x) \sin(\mu y) \\ V_{mn} \sin(\lambda x) \cos(\mu y) \\ W_{mn} \sin(\lambda x) \sin(\mu y) \\ \Theta_{mn} \sin(\lambda x) \sin(\mu y) \end{Bmatrix} \tag{36}$$

where $(U_{mn}, V_{mn}, W_{mn}, \Theta_{mn})$ are the unknown maximum displacement coefficients.

Table 1. Fiber thermo-mechanical properties used in this study [10].

Fiber	T300	HMS	P100
E_1 (GPa)	233.13	379.35	796.63
E_2 (GPa)	23.11	6.21	7.24
G_1 (GPa)	8.97	7.59	6.9
G_2 (GPa)	8.28	2.21	2.62
ν_1	0.2	0.2	0.2
ν_2	0.4	0.4	0.4
$\alpha_1 (10^{-6}/C°)$	-0.54	-0.99	-1.40
$\alpha_2 (10^{-6}/C°)$	10.08	6.84	6.84

Table 2. Matrix thermo-mechanical properties used in this study [10].

Matrix	E (GPa)	G (GPa)	ν	α $(10^{-6}/C°)$
Epoxy 5208	4.35	1.59	0.37	43.92
Epoxy CE339	4.35	1.59	0.37	63.36
Aluminum 2024	73.11	27.58	0.33	23.22

The same solution is used for the external applied loading: mechanical distribution load q, and thermal load T:

$$\begin{Bmatrix} q \\ T_0 \\ T_1 \end{Bmatrix} = \sum_{m=1}^{\infty} \sum_{n=1}^{\infty} \begin{Bmatrix} q_{mn} \\ \bar{T}_0 \\ \bar{T}_1 \end{Bmatrix} \sin(\lambda x) \sin(\mu y) \tag{37}$$

Substituting Eq. (36) and (37) into Eqs. (32), the following analytical solutions are obtained:

$$\begin{bmatrix} a_{11} & a_{12} & a_{13} & a_{14} \\ a_{12} & a_{22} & a_{23} & a_{24} \\ a_{13} & a_{23} & a_{33} & a_{34} \\ a_{14} & a_{24} & a_{34} & a_{44} \end{bmatrix} \begin{Bmatrix} U_{mn} \\ V_{mn} \\ W_{mn} \\ \Theta_{mn} \end{Bmatrix} = \begin{Bmatrix} P_1^T \\ P_2^T \\ P_3^T \\ P_4^T \end{Bmatrix} \tag{38}$$

where,

$$a_{11} = (A_{11}\lambda^2 + A_{66}\mu^2); a_{12} = \lambda\mu(A_{12} + A_{66}); a_{13} = -\lambda(B_{11}\lambda^2 + (B_{12} + 2B_{66})\mu^2);$$

$$a_{14} = \lambda(k_1 A' B_{11}^s \lambda^2 + k_2 B' B_{12}^s \mu^2 - (k_1 A' + k_2 B')B_{66}^s \mu^2 - L_{13}); \quad a_{22} = (A_{66}\lambda^2 + A_{22}\mu^2); a_{23} = -\mu(B_{22}\mu^2 + (B_{12} + 2B_{66})\lambda^2);$$

$$a_{24} = \mu(k_2 B' B_{22}^s \mu^2 + k_1 A' B_{12}^s \lambda^2 - (k_1 A' + k_2 B')B_{66}^s \lambda^2 - L_{23}); \quad a_{33} = (D_{11}\lambda^4 + 2(D_{12} + 2D_{66})\lambda^2\mu^2 + D_{22}\mu^4);$$

$$a_{34} = -(k_1 A')\lambda^2(D_{11}^s \lambda^2 + D_{12}^s \mu^2) - 2(k_1 A' + k_2 B')D_{66}^s \lambda^2\mu^2 - (k_2 B')\mu^2(D_{12}^s \lambda^2 + D_{22}^s \mu^2) + L_{13}^\alpha \lambda^2 + L_{23}^\alpha \mu^2;$$

$$a_{44} = -k_1(H_{11}^s k_1 A'\lambda^2 + H_{12}^s k_2 B'\mu^2) + (k_1 A' + k_2 B')^2 H_{66}^s \lambda^2\mu^2 - k_2(H_{12}^s k_1 A'\lambda^2 + H_{22}^s k_2 B'\mu^2) + (k_1 A')^2 A_{55}^s \lambda^2 + (k_2 B')^2 A_{44}^s \mu^2 - (k_1 A')\lambda^2 Z_{13} - (k_2 B')\mu^2 Z_{23} + Z_{33} + k_1 Y_{13} + k_2 Y_{23} + \mu^2 AL_{44}^s + \lambda^2 AL_{55}^s + 2(k_1 A'\lambda^2 AL_{55} + k_2 B'\mu^2 AL_{44}); \tag{39}$$

$$P_1^T = \lambda(A_1^T \bar{T}_0 + B_1^T \bar{T}_1); \quad P_2^T = \mu(A_2^T \bar{T}_0 + B_2^T \bar{T}_1); \quad P_3^T = -q_0 - \lambda^2(B_1^T \bar{T}_0 + D_1^T \bar{T}_1) - \mu^2(B_2^T \bar{T}_0 + D_2^T \bar{T}_1);$$

$$P_4^T = -k_1(Bs_1^T \bar{T}_0 + Ds_1^T \bar{T}_1) - k_2(Bs_2^T \bar{T}_0 + Ds_2^T \bar{T}_1) - L_{33}^T \bar{T}_0 - L_{33}^{\alpha T} \bar{T}_1$$

where,

$$(A_i^T \quad B_i^T \quad D_i^T \quad Bs_i^T \quad Ds_i^T) = \int_{-h/2}^{h/2} \bar{Q}_{i6} \begin{Bmatrix} \alpha_x \\ \alpha_y \\ \alpha_z \end{Bmatrix} (1 \quad z \quad z^2 \quad f(z) \quad zf(z))Tdz \tag{40a}$$

and

$$(L_{33}^T \quad L_{33}^{\alpha T}) = \int_{-h/2}^{h/2} \bar{Q}_{3x6} \begin{Bmatrix} \alpha_x \\ \alpha_y \\ \alpha_z \end{Bmatrix} (1 \quad g'(z))g'(z)Tdz \tag{40b}$$

4. Numerical Results and Discussion

The present subsection provides an assortment of numerical demonstrations that illustrate the critical role of micromechanics-based models in estimating the thermo-mechanical characteristics of laminated composite plates. Detailed comparison and synthesis analyses are offered, and findings from other studies collected from the current literature are stated. The thermo-mechanical properties of the used matrix and fibers are shown in Tables 1 and 2, respectively.

The dimensionless parameters are given in the following normalized form to demonstrate the point:

$$\hat{w} = \left[\frac{q_0 a^4}{h^3 \beta} + \frac{\alpha_1 \bar{T}_2 a^2}{10h}\right]^{-1} w(\frac{a}{2}, \frac{b}{2}, 0) \text{ with } \beta = \frac{\pi^4}{12}\left[4G_{12} + \frac{E_1 + (1+v_{12})E_2}{1-v_{12}v_{21}}\right]; \quad \overline{w} = \frac{100h^3 E_2}{a^4 q_0} w(\frac{a}{2}, \frac{b}{2}, 0); \quad \overline{w}_{Th} = \frac{10h}{\alpha_1 a^2 T_1} w(\frac{a}{2}, \frac{b}{2}, 0);$$

$$(\bar{\sigma}_x, \bar{\sigma}_y, \bar{\sigma}_z, \bar{\tau}_{xy}) = \frac{h^2}{a^2 q_0}(\sigma_x, \sigma_y, \sigma_z, \tau_{xy}); (\bar{\tau}_{xz}, \bar{\tau}_{yz}) = \frac{h}{aq_0}(\tau_{xz}, \tau_{yz}); \tag{41}$$

$$(\bar{\sigma}_x, \bar{\sigma}_y, \bar{\sigma}_z, \bar{\tau}_{xy})_{Th} = \frac{10h}{\alpha_1 a^2 E_2 T_1}(\sigma_x, \sigma_y, \sigma_z, \tau_{xy})_{Th}; (\bar{\tau}_{xz}, \bar{\tau}_{yz})_{Th} = \frac{1}{\alpha_1 E_2 T_1}(\tau_{xz}, \tau_{yz})_{Th}$$

4.1. Validation and evaluation

This section aims to compare and validate the obtained results from the developed Quasi-3D theory with those from other theories and models. The goal is to evaluate the accuracy and reliability of the present theory. The material characteristics of each layer of the laminated plate in this specific subsection are as follows [29, 36-38]:

$$\frac{E_1}{E_2} = 25 \; ; \; E_3 = E_2 \; ; \; \frac{G_{12}}{E_2} = 0.5 \; ; \; \frac{G_{13}}{E_2} = 0.5 \; ; \; \frac{G_{23}}{E_2} = 0.2 \; ; \; \nu_{12} = 0.25 \; ; \; \nu_{23} = \nu_{13} = \nu_{12}, \; \frac{\alpha_1}{\alpha_2} = \frac{1}{3} \; ; \; \frac{\alpha_1}{\alpha_3} = \frac{1}{3} \qquad (42)$$

The dimensionless transversal displacement of simply supported antisymmetric [0°/90°] laminated composite plates under a combined sinusoidal thermo-mechanical load is illustrated in Table 3. It is seen that the obtained results present a good agreement with those given by using other shear deformation laminated plate theories concerning various length-to-thickness ratios. It should be noted that the first-order laminated plate theory requires an appropriate shear correction factor for shear stress. This factor depends on various parameters, such as geometry, material properties, and imposed boundary conditions. More operations are then required to predict the mechanical behaviors of this class of structures. The computations provided by Zuo et al. [45], and Reddy and Hsu [67] are founded on the first shear deformation laminated plate, which overestimates the deflection of thick laminated plates. In Zenkour [29], various higher-order shear deformation laminated plate theories are formulated based on both sinusoidal and parabolic shape functions. These ensure traction-free boundary conditions at the top and bottom surfaces of the laminated plate. The theory used in this study generates five independent unknowns. Zuo et al. [43] also proposed a wavelet finite element formulation based on Reddy's laminated theory. The accuracy of this simulation is determined by the number of normalized coordinates relative to the B-spline functions and the use of scaling functions that are complex in computer implementation. The results given by Garg et al. [36] are derived using the trigonometric zigzag theory, which is cumbersome and computationally expensive. Chattibi et al. [50] utilized refined four-variable shear deformation laminated plate theory with sinusoidal distribution for both strains and stress across thickness coordinate. Joshan et al. [37] expressed an inverse hyperbolic shear deformation theory to predict the deflection of laminated plates using five unknowns. Similarly, Joshan et al. [38] reduced the number of unknowns by introducing undetermined integral variables to calculate the deflection of laminated plates. The aforementioned theories overlook the thickness stretching effect, a significant factor, particularly in thick laminated plates. This effect enhances the stiffness and strength of the laminated plates, it should be considered when the thickness of laminated plates is important and can help in optimizing design and preventing failure if addressed properly. In this context, Ameri et al. [51] introduced efficient shear deformation laminated plate theories that account for the thickness stretching effect. The present theory demonstrates the same efficiency and precision. It can be also observed that the deflection decreases when the slenderness ratio increases. The second example focuses on simply supported laminated plates subjected to sinusoidal thermal loading across a range of slenderness ratios. Table 4 offers a comparative study of the obtained results with those reported by other shear deformation laminated plate theories. A closer inspection of Table 4 confirms the validity and precision of the obtained dimensionless deflections. Importantly, other higher-order shear deformation theories generate a host of unknowns without introducing thickness stretching. Moreover, the deflection of laminated composite plates under thermal loading depends on various factors, such as the CTE, the stacking sequence of the composite, and the robustness of the used theory to investigate the thermal behavior of laminated composite plates. For this load case, the CTE can vary across the different layers using arbitrary coefficients. The occurrence of those variations might result in differential thermal expansion, leading to the possibility of generating internal deflection within the laminated plate. Consequently, the determined magnitudes of stress and strain could be overestimated since the plate is subjected to thermal loading. A comprehensive analysis is often necessary and is typically required to predict accurately the behavior of laminated composite plates under thermal loading. As observed, the deflection of laminated plates under thermal loading is expected to decrease gradually with increasing slenderness ratio.

The subsequent example examines laminated composite plates subjected to mechanical loading across different slenderness ratios. Table 5 compares the obtained dimensionless deflections with those from other laminated plate theories. After inspection of the obtained results, the present formulation demonstrates that the same efficiency is viewed, including the thickness stretching, which contributes to enhancing the accuracy and precision of the developed shear deformation theory with only four unknowns and integrating the undetermined integral terms. Recall that both first and higher-order shear deformation laminated theories omit the stretching effect, often leading to overestimation of deflection in thick laminated composite plates compared to 3D solutions by Pagano [68]. To avoid this limitation, the present theory retains a hyperbolic variation for out-of-plan normal strain, in which this assumption makes a bridge between 2D higher-order shear deformation theory and 3D elasticity considerations. As can be observed, the dimensionless deflection decreases as the slenderness ratio increases and a high magnitude of deflection is observed for a very high thickness case. Additionally, the dimensionless stresses of simply supported laminated plates under sinusoidal mechanical loading with two slenderness ratios (a/h=10 and a/h=4) are assessed in comparison with results from other theories. The numerical results are presented in Table 6. The obtained results are in good agreement with those given by Reddy [69] and Joshan et al. [37], based on higher-order shear deformation theory, and Ameri et al. [51] by using Quasi-3D higher-order shear deformation theory, and exact elastic solutions given by Pagano [68]. As previously noted, the compared results are founded on the new integral shear deformation laminated plate theory that has only four unknowns and retains the thickness stretching. Once again, this example demonstrates the efficiently and accuracy of the formulated theory in stress analysis of thicker laminated composite plates. As highlighted in this example, the chosen stacking sequence [0°/90°] results in a symmetrical distribution of transverse stresses and an asymmetrical distribution of normal stresses. This observation can be considered a critical parameter in estimating the mechanical behavior of laminated composite plates. It can be optimized to improve strength, stiffness, delamination resistance, and fatigue resistance.

4.2. Parametric analysis

The accurateness of thermo-mechanical characteristics relies on the utilization of these micromechanical models, as mentioned earlier. It is essential to acknowledge that in a thermo-mechanical analysis, the mechanical and thermal parameters are coupled. Any variation to these models based on micromechanics has a direct impact on the performance of laminated composite plates. These models analyze the material properties of each layer, enabling a detailed examination of the behavior of the composite. Through systematic optimization of these parameters, researchers may expose the complexities of the thermo-mechanical characteristics, facilitating the development of laminated composite plates that satisfy the most favorable thermal and mechanical performance requirements. The aforementioned accuracy, in return, promotes the development of composite materials that are more efficient, durable, and reliable. The significance of micromechanical analysis in comprehending the thermo-mechanical characteristics of laminated composite plates cannot be underestimated, rendering it a crucial study domain for diverse sectors.

Table 3. Comparisons of dimensionless deflection parameters $\hat{w}$ of simply supported laminated [0°/90°] composite plates under combined sinusoidal thermal and mechanical loading with other theories and various slenderness ratios ($q_0 = 100$; $\overline{T_1} = 100$; $\alpha_1 = 10^{-6}$).

Theories	a/h							
	5	6.5	10	12.5	20	25	50	100
Zuo et al. [45] First-order plate theory	4.0420	3.4671	2.8443	2.7005	2.5448	2.5089	2.4609	2.4488
Reddy and Hsu [67]	4.0415	3.4666	2.8438	2.7001	2.5443	2.5083	2.4597	2.4541
Joshan et al. [37]	3.6797	3.2433	2.7602	2.6471	2.5240	2.4955	2.4574	2.4478
Zenkour [29] Sinusoidal plate theory	3.7821	3.3090	2.7859	2.6636	2.6636	2.4996	2.4584	2.4481
Zenkour [29] Higher order plate theory	3.8120	3.3273	2.7927	2.6679	2.5321	2.5006	2.4586	2.4481
Joshan et al. [38]	3.8302	3.3362	2.7950	2.6692	2.5325	2.5009	2.4587	2.4482
Ameri et al. [51]	3.7384	3.2768	2.7714	2.6540	2.5264	2.4969	2.4576	2.4477
Zuo et al. [45] Higher-order plate theory	3.8320	3.3375	2.7956	2.6697	2.5329	2.5013	2.4590	2.4484
Garg et al. [36]	3.8732	3.3608	2.8033	2.6742	2.5343	2.5019	2.4588	2.4481
Chattibi et al. [50]	3.8013	3.3186	2.7885	2.6650	2.5309	2.4999	2.4585	2.4481
Present	3.7581	3.2887	2.7757	2.6566	2.5273	2.4974	2.4575	2.4476

Table 4. Comparisons of dimensionless deflection parameters $\overline{w}_{Th}$ of simply supported laminated [0°/90°] composite plates under sinusoidal thermal loading with other theories and various slenderness ratios ($\overline{T_1} = 100$).

Theories	a/h							
	5	6.5	10	12.5	20	25	50	100
Joshan et al. [37]	1.6955	1.6888	1.6814	1.6796	1.6777	1.6773	1.6767	1.6766
Joshan et al. [38]	1.6894	1.6848	1.6798	1.6786	1.6773	1.677	1.6767	1.6766
Reddy and Hsu [67]	1.6765	1.6765	1.6765	1.6765	1.6765	1.6765	1.6765	1.6765
Zenkour [29] Sinusoidal plate theory	1.6894	1.6848	1.6798	1.6786	1.6773	1.677	1.6767	1.6766
Zenkour [29] Higher order plate theory	1.691	1.6858	1.6802	1.6789	1.6774	1.6771	1.6767	1.6766
Mechab et al. [47]	1.6896	1.6849	1.6798	1.6786	1.6773	1.677	1.6767	1.6766
Ameri et al. [51]	1.6877	1.6843	1.6806	1.6796	1.6783	1.6778	1.6789	1.6766
Garg et al. [36]	1.6845	1.6818	1.6786	1.6778	1.677	1.6768	1.6765	1.6764
Chattibi et al. [50]	1.6910	1.6858	1.6802	1.6789	1.6774	1.6771	1.6767	1.6766
Present	1.6843	1.6810	1.6783	1.6777	1.6772	1.6771	1.6773	1.6775

Table 5. Comparisons of dimensionless deflection parameters $\overline{w}$ of simply supported laminated [0°/90°] composite plates under sinusoidal mechanical loading with other theories and various slenderness ratios ($q_0 = 100$).

Theories	a/h				
	2	5	10	20	100
Joshan et al. [38]	4.5629	1.6671	1.2161	1.1018	1.0651
Pagano [68]	4.9362	1.7287	1.2318	1.1060	1.0742
Mindlin [70]	5.4103	1.7627	1.2416	1.1113	1.0653
Reddy [69]	4.5619	1.6670	1.2161	1.1018	1.0651
Kim et al. [71]	4.5619	1.6670	1.2161	1.1018	1.0651
Ameri et al. [51]	4.3401	1.6264	1.2057	1.0991	1.0649
Present	4.4270	1.6351	1.2076	1.0996	1.0649

4.2.1. The impact of micromechanics-based models on the mechanical behavior of laminated plates

To assess the impact of micromechanics-based models on the dimensionless deflection of laminated composite plates, various homogenization schemes are considered, namely: Rule of the mixture, Chamis, and Hill-Hashin-Christensen-Lo micromechanics-based models. In addition, to perform a reliable analysis, various fiber-reinforced material systems are utilized, for carbon fibers: T300, High Modulus Strength (HMS), and P100, for embedded matrix, the same Epoxy matrix is used for convenience. Table 7 presents benchmark results on the dimensionless deflection of fiber-reinforced composite plates subjected to sinusoidal load, considering different fiber volume fractions and slenderness ratios. As the fractions increase, the deflections decrease, highlighting the enhanced strength and stiffness of the composite due to higher fiber concentration. The P100/Epoxy system has exceptional rigidity with minimal deflection, while the T300/Epoxy system tends to exhibit greater deflection. From a modeling perspective, both the Rule of Mixture Model and the Chamis Model yield almost identical effective elastic properties for composites.

The Rule of Mixture Model assumes consistent thicknesses for the fibers and matrix, embedding the fibers within a rectangular plate matrix. On the other hand, the Chamis Model takes a more detailed approach by dividing the composite into multiple subregions. This leads to comparable deflections that vary slightly when the fiber volume fraction is changed. The HHCL Model presents a different approach, where the composite is represented as a cylindrical matrix filled with cylindrical fibers. This model places a significant emphasis on the transverse shear modulus and predicts significantly higher deflections, which increase as the fiber fractions increase. The slenderness ratio of the plate is an important factor. Thicker plates tend to have higher deflection compared to thin plates because the transversal stresses are reduced in the slender plates. This reduction in transversal stresses renders the shear properties less significant in models based on micromechanics. Significantly, composites that have a higher amount of fiber are at a higher possibility of producing imperfections such as cracks and delamination, which might potentially influence the assessment of deflection. This highlights the significance of comprehending the basic limitations of these models and promoting the moderate deployment or investigation of more advanced techniques when considered relevant.

4.2.2. The impact of micromechanics-based models on the thermal behavior of laminated plates

The following example investigates how various micromechanics-based models, including Van Fo Fy, Schapery, Chamberlain, Schneider, and Chamis, influence the dimensionless deflection of laminated composite plates under thermal loading. The analysis considers two fiber-reinforced material systems: T300/Epoxy and P100/Epoxy. Table 8 presents the variation of the dimensionless deflection as a function of fiber volume fraction for various slenderness ratios. For convenience, the rule of the mixture is employed to derive the effective elastic constants. It is important to note that deflections tend to decrease as the volume fraction of fibers increases. This occurrence can be related to the fact that the matrix material has a higher CTE in comparison with the fibers. Here,

the matrix is more thermally sensitive, and this sensitivity rate to thermal bending is governed by the homogenized CTE of the laminated plates. In this case, each micromechanics-based model has its assumptions, and the selection of a model is dependent on the complexity of the composite material and the required level of analysis precision. Schneider, Chamberlain, and Chamis models assume identical longitudinal CTE, aligning with the Schapery model. For the transverse CTE, thermal deflections show marginal differences at high fiber volume fractions. This is because both Schapery's and Chamis's models predict the transverse CTE to be directly proportional to the fiber volume fraction. Thus, the deflections change with a slight increment when the slenderness ratio increases. The Chamberlain model appears more sensitive to deflection and presents contradictory magnitude when the fiber volume fraction increases to 100%. It is remarkable that all micromechanics-based models consistently exhibit even magnitude across various preferred and average fiber volume fractions ([40% to 60%] for T300/Epoxy and [20% to 60%] for P100/Epoxy laminates). However, fiber reinforcement can also influence the composite material's CTE, specifically, if the fibers have a negative CTE (P100 and T300). For instance, in situations where fibers such as P100 and T300 exhibit a negative coefficient of thermal expansion (CTE), it can balance the positive CTE of the matrix material. As a result, this leads to a reduction in the overall CTE of the composites.

In another situation, when a temperature change is applied through the laminated plate thickness, the differential expansion and contraction of its constituent materials can cause thermal stresses within the laminated plate. These stresses can deform, buckle, or even fracture the laminated plate. Factors like the orientation of fibers, their volume fraction, and used homogenization model can affect the magnitude and direction of thermal stresses, as well as the overall response of the laminated plate to thermal loading. Specifically, if the fibers have a low CTE and are in their optimal orientation with the direction of the thermal stresses, they can aid in mitigating the thermal stresses and reducing the laminated plate's sensitivity to laminated problems (delamination, fiber buckling...). This scenario might be detrimental in applications where temperature sensitivity is vital during mechanical loading.

Table 6. Comparisons of dimensionless stresses for simply supported laminated composite plates [0°/90°] under sinusoidal mechanical loading with other theories.

a/h	Theories	$\overline{\sigma}_x\left(\frac{a}{2},\frac{b}{2},\frac{h}{2}\right)$	$\overline{\sigma}_y\left(\frac{a}{2},\frac{b}{2},\frac{h}{2}\right)$	$\overline{\sigma}_z\left(\frac{a}{2},\frac{b}{2},\frac{h}{2}\right)$	$\overline{\tau}_{xy}\left(0,0,\frac{h}{2}\right)$	$\overline{\tau}_{xz}\left(0,\frac{b}{2},0\right)$	$\overline{\tau}_{yz}\left(\frac{a}{2},0,0\right)$
4	Mindlin [70]	0.7157	0.0843	/	0.0525	/	/
	Joshan et al. [38]	0.9060	0.0891	/	0.0577	0.3128	0.3128
	Reddy [69]	0.9060	0.0891	/	0.0577	0.3128	0.3128
	Pagano [68]	0.8410	0.1090	/	0.0591	0.3210	0.3130
	Ameri et al. [51]	0.8949	0.0899	0.0048	0.0573	0.3022	0.3022
	Present	0.8866	0.0888	0.0047	0.0573	0.2971	0.2971
10	Mindlin [70]	0.7157	0.0843	/	0.0525	/	/
	Joshan et al. [38]	0.7468	0.0851	/	0.0533	0.3190	0.3190
	Reddy [69]	0.7468	0.0851	/	0.0533	0.3190	0.3190
	Pagano [68]	0.7302	0.0886	/	0.0535	0.3310	0.3310
	Ameri et al. [51]	0.7450	0.0854	0.0017	0.0532	0.3083	0.3083
	Present	0.7425	0.0843	0.0016	0.0533	0.3014	0.3014

Table 7. Micromechanical analysis of dimensionless deflections $\overline{w}$ for simply supported laminated composite plates [0°/90°] under sinusoidal mechanical loading with various slenderness ratios and fiber volume fractions. ($q_0 = 100$).

a/h	composite	Micromechanics-based model	V_f				
			10	25	50	75	90
5	T300/Epoxy	ROM	2.4568	2.1226	1.9021	1.9083	2.0117
		Chamis	2.5345	2.2751	2.0926	2.0622	2.0942
		Hill-Hashin-Christensen-Lo	2.6321	2.3427	2.1957	2.3008	2.5071
	HMS/Epoxy	ROM	2.1985	1.6881	1.2679	1.0111	0.8698
		Chamis	2.1437	1.6410	1.2162	0.9618	0.8396
		Hill-Hashin-Christensen-Lo	1.9016	1.7373	1.7395	1.9864	2.2991
	P100/Epoxy	ROM	1.8127	1.2881	0.9597	0.7894	0.7010
		Chamis	1.8178	1.2996	0.9529	0.7704	0.6867
		Hill-Hashin-Christensen-Lo	1.7310	1.4202	1.3354	1.4918	1.7214
10	T300/Epoxy	ROM	2.0223	1.6976	1.4859	1.4934	1.5952
		Chamis	2.0995	1.8461	1.6707	1.6433	1.6761
		Hill-Hashin-Christensen-Lo	2.1467	1.8650	1.7160	1.7920	1.9534
	HMS/Epoxy	ROM	1.7800	1.3039	0.9351	0.7385	0.6452
		Chamis	1.7518	1.2933	0.9252	0.7228	0.6331
		Hill-Hashin-Christensen-Lo	1.5847	1.3953	1.3349	1.4772	1.6841
	P100/Epoxy	ROM	1.4057	0.9161	0.6300	0.5069	0.4571
		Chamis	1.4293	0.9532	0.6540	0.5142	0.4575
		Hill-Hashin-Christensen-Lo	1.3875	1.0634	0.9301	0.9997	1.1398
100	T300/Epoxy	ROM	1.9627	1.5970	1.3721	1.3832	1.4964
		Chamis	2.0585	1.7625	1.5722	1.5468	1.5866
		Hill-Hashin-Christensen-Lo	2.0823	1.7584	1.5939	1.6651	1.8234
	HMS/Epoxy	ROM	1.6909	1.1907	0.8277	0.6495	0.5726
		Chamis	1.6756	1.1965	0.8345	0.6465	0.5672
		Hill-Hashin-Christensen-Lo	1.5356	1.3105	1.2164	1.3210	1.4938
	P100/Epoxy	ROM	1.2874	0.7927	0.5187	0.4115	0.3747
		Chamis	1.3216	0.8404	0.5535	0.4277	0.3802
		Hill-Hashin-Christensen-Lo	1.2996	0.9505	0.7948	0.8340	0.9438

Table 8. Micromechanical analysis of dimensionless deflections $\bar{w}_{Th}$ for simply supported laminated composite plates [0°/90°] under sinusoidal thermal loading with various slenderness ratios and fiber volume fractions ($\overline{T}_1 = 100$).

a/h	Composite	Micromechanics-based model	V_f					
			0	0.20	0.40	0.60	0.80	1
5	T300/Epoxy	Van Fo Fy	1.0120	0.5059	0.4873	0.4801	0.4750	0.4626
		Schapery	1.0120	0.5057	0.4871	0.4801	0.4755	0.4671
		Chamberlain	1.0120	0.5183	0.4941	0.4802	0.4385	0.5508
		Schneider	1.0120	0.5103	0.4913	0.4802	0.4690	0.4380
		Chamis	1.0120	0.5199	0.4923	0.4802	0.4723	0.4671
	P100/Epoxy	Van Fo Fy	1.0120	0.4640	0.4529	0.4439	0.4279	0.3718
		Schapery	1.0120	0.4640	0.4528	0.4435	0.4266	0.3618
		Chamberlain	1.0120	0.4616	0.4407	0.4080	0.2023	0.5968
		Schneider	1.0120	0.4632	0.4460	0.4271	0.3983	0.2754
		Chamis	1.0120	0.4608	0.4417	0.4259	0.4041	0.3618
10	T300/Epoxy	Van Fo Fy	0.9731	0.4966	0.4802	0.4736	0.4677	0.4527
		Schapery	0.9731	0.4964	0.4801	0.4735	0.4682	0.4572
		Chamberlain	0.9731	0.5089	0.4870	0.4737	0.4313	0.5405
		Schneider	0.9731	0.5010	0.4842	0.4736	0.4617	0.4282
		Chamis	0.9731	0.5105	0.4853	0.4736	0.4650	0.4572
	P100/Epoxy	Van Fo Fy	0.9731	0.4614	0.4522	0.4434	0.4270	0.3703
		Schapery	0.9731	0.4614	0.4521	0.4431	0.4258	0.3603
		Chamberlain	0.9731	0.4590	0.4400	0.4078	0.2027	0.5937
		Schneider	0.9731	0.4606	0.4453	0.4267	0.3977	0.2745
		Chamis	0.9731	0.4583	0.4410	0.4255	0.4034	0.3603
100	T300/Epoxy	Van Fo Fy	0.7153	0.4309	0.4312	0.4278	0.4160	0.3815
		Schapery	0.7153	0.4307	0.4311	0.4278	0.4166	0.3860
		Chamberlain	0.7153	0.4431	0.4380	0.4280	0.3800	0.4680
		Schneider	0.7153	0.4353	0.4352	0.4279	0.4101	0.3574
		Chamis	0.7153	0.4446	0.4362	0.4279	0.4134	0.3860
	P100/Epoxy	Van Fo Fy	0.7153	0.4452	0.4514	0.4470	0.4301	0.3689
		Schapery	0.7153	0.4451	0.4513	0.4466	0.4289	0.3590
		Chamberlain	0.7153	0.4423	0.4348	0.3787	0.7788	0.5198
		Schneider	0.7153	0.4443	0.4445	0.4303	0.4008	0.2734
		Chamis	0.7153	0.4420	0.4403	0.4291	0.4065	0.3590

To investigate the impact of thermal micromechanics-based models on the thermo-mechanical behavior of laminated plates, the next example is performed to laminate composite plates under thermo-mechanical loading. Table 9 illustrates the obtained dimensionless deflections as a function of fiber volume fraction for various slenderness ratios and under both thermal and mechanical loading. The effects of mechanical loading on the laminated plate are more pronounced than thermal loading. Significant dimensionless deflections occur around specific fiber volume fractions ([around 60%] for T300/Epoxy and [around 80%] for P100/Epoxy laminates) for all used slenderness ratios. These deflection values can be used to identify the fiber volume fraction at which the laminated composite plate exhibits maximum stiffness and strength and to provide an optimal balance between the resistance and stiffness of the composite material system. It is also shown that the Chamberlain model yields higher values with a slight difference compared to the other models, and the influence of mechanical loading is confirmed through a closer inspection of the obtained values. It is also confirmed that the preformed material system of laminated composite plates can influence their stiffness, strength, CTE, and response to thermal and mechanical loading. For specific applications, it is critical to consider the properties and behavior of the fibers, especially the fiber stacking sequences.

4.2.3. The effect of stacking sequence on thermomechanical behavior of laminated plates

Another study was conducted to explore the effect of stacking sequence on the thermo-mechanical response of simply supported laminated composite plates with various fiber volume fractions and a slenderness ratio a/h=10. Table 10 presents dimensionless deflections of simply supported laminated composite plates with various fiber stacking sequences as a function of fiber volume fractions. As observed, both fiber stacking sequences and the selected micromechanics-based model for predicting CTE influence the dimensionless deflections. The fiber volume fraction contributes to the increase in dimensionless deflections as the number of fibers increases until a high magnitude is marked by V_f=60%, and then the dimensionless deflections continue to decrease. It is also observed that an optimum cross-stacking of fibers provides a high resistance compared to the other used fiber stacking sequences. Dimensionless deflections predicted by thermal micromechanics-based models differ slightly. Each model's assumptions make this expected. It is vital to note that the behavior of these models, especially in reaction to fiber volume fraction changes, is consistent. The rule of mixture model for elastic constants confirms that mechanical impacts dominate thermal ones in laminate behavior. Table 11 displays the dimensionless deflections of simply supported composite laminated plates under thermal loading with various fiber volume fractions and fiber stacking sequences. Various micromechanics-based models are considered. In contrast to thermo-mechanical behavior, the cross-fiber stacking sequence contributes to an increase in the dimensionless deflections, because the stacking sequence can influence the CTE of the laminated composite plate, and thus the amount of thermal expansion. Different fiber orientations between adjacent plies in a laminated composite plate increase the risk of delamination. The process of delamination can significantly reduce both the strength and stiffness of the material. In situations with consistent fiber alignment, the composite material presents an increased level of rigidity and resistance in the same direction as the fibers. A uniform fiber direction in the material ensures more predictable CTE values compared to laminate in a cross-ply configuration. About the Chamberlain micromechanics-based model, observations indicate that an increase in the fiber volume fraction leads to a decrease in the dimensionless deflections. On the contrary, alternative micromechanical models suggest that dimensionless deflections decrease until a fiber volume fraction of 80% after these deflections begin to increase as the laminated plate mainly reveals the thermo-mechanical characteristics of the fibers. It is imperative to emphasize that the matrix material generally exhibits a more apparent positive longitudinal CTE compared to the fibers. In certain cases, fibers might show a

longitudinal CTE that is negative. As a result, the ultimate coefficient of CTE of the laminated composite plate may exhibit variability, potentially exceeding or decreasing under the basic CTE of the matrix material. The outcome of this is dependent upon the amount of the volume fraction and the arrangement of the fibers in the stacking sequence. This observation clarifies the varying values seen when laminated plates fully reflect fiber characteristics (V_f =100%) related to the micromechanics-based models that are dependent on more than just the fiber volume fraction alone. Besides longitudinal thermal expansion, the transverse CTE of a laminated composite can have a significant impact on its thermo-mechanical behavior.

4.2.4. The impact of micromechanics-based models on thermomechanical stress of laminated plates

The matrix and fibers of the laminate could exhibit a mismatch in their transverse thermal expansion. This can cause transverse thermal stresses within the laminated composite plates that can lead to delamination or cracking. The magnitude of transverse stresses is determined by the difference between the transverse CTE of the matrix and fibers, as well as the degree of interlaminar constraint. This discrepancy offers insights into the internal stresses within laminated composite plates. Figure 2 illustrates the distribution of dimensionless transverse stress $\bar{\tau}_{yz}$ through the thickness coordinate for T300/Epoxy laminated composite plates [0°/90°] under mechanical loading with various fiber volume fractions, and micromechanics-based models (a/h=10). For low fiber volume fractions, it is observed that both the rule of the mixture and the Chamis models generate a relatively symmetric distribution of transverse stress to the mid-plane of the composite plate. The HHCL model produces an asymmetric stress distribution at the mid-plane of the laminated plate, the stress distribution changes from maximum tensile stress at the laminated plate's mid-plane to vanished stress in the top and bottom surface of the laminated plate. The same distribution is observed in the average fiber volume fraction. Considering the high fiber volume fraction, the Chamis model displays a uniform and symmetrical distribution, whereas the HHCL model exhibits an asymmetrical distribution caused by variations in fiber orientations and the resulting stress characteristics, unlike the rule of mixture. Figures 3 and 4 depict similar trends of dimensionless transverse stress for HMS/Epoxy and P100/Epoxy laminated composite plates, respectively. Visual inspection of the plotted figures reveals significant discontinuities in the transverse stress values at the ply interfaces, in the laminated composite plates' mid-planes. The Chamis model provides lower and higher variations of the transverse stress in the lower and upper plies, respectively. The rule of mixture presents an inverse distribution compared to Chamis' model. As the fiber volume fraction increases, the HHCL model reduces the variation of the transverse stress at the laminate composite plate's mid-plane. This is because P100 and HMS fibers are typically stronger and stiffer compared to T300 fiber, and the HHCL micromechanics-based model can predict the effective elastic properties of laminated composites accurately, especially for materials with anti-symmetric layups. To predict the overall properties of the laminate, the model includes a micromechanics-based approach that takes into account the properties and orientations of the individual plies. In one aspect, the orientation of the fibers is becoming increasingly important in determining composite mechanical behavior. Therefore, design considerations should account for this specific orientation to optimally utilize its desired mechanical characteristics and improve the performance of the composite material. The selection of a suitable micromechanical model is crucial for effectively achieve a strong connection between plies and maintain appropriate variation in interlaminar shear stresses. Additionally, adopting a structural design that minimizes stress concentrations and facilitates the even distribution of loads among the layers can greatly enhance the potential of a laminated composite plate to resist delamination.

Table 9. Micromechanical analysis of dimensionless deflections $\overline{w}$ for simply supported laminated composite plates [0°/90°] under sinusoidal thermo-mechanical loading with various slenderness ratios and fiber volume fractions ($\overline{T}_1 = 100$, $q_0 = 100$).

a/h	Composite	Micromechanics-based model	V_f					
			0	0.20	0.40	0.60	0.80	1
5	T300/Epoxy	Van Fo Fy	0.9180	2.2636	2.8324	3.0018	2.8414	2.2870
		Schapery	0.9180	2.2635	2.8321	3.0014	2.8406	2.2860
		Chamberlain	0.9180	2.2657	2.8373	3.0090	2.8493	2.2937
		Schneider	0.9180	2.2646	2.8360	3.0070	2.8456	2.2892
		Chamis	0.9180	2.2659	2.8366	3.0062	2.8439	2.2860
	P100/Epoxy	Van Fo Fy	0.9180	4.2666	5.5506	6.2017	6.3555	5.9191
		Schapery	0.9180	4.2667	5.5510	6.2029	6.3577	5.9224
		Chamberlain	0.9180	4.2782	5.5803	6.2478	6.4096	5.9679
		Schneider	0.9180	4.2718	5.5720	6.2344	6.3842	5.9355
		Chamis	0.9180	4.2802	5.5790	6.2356	6.3809	5.9224
10	T300/Epoxy	Van Fo Fy	0.7842	1.8252	2.2263	2.3397	2.2310	1.8397
		Schapery	0.7842	1.8251	2.2262	2.3393	2.2304	1.8390
		Chamberlain	0.7842	1.8269	2.2303	2.3453	2.2373	1.8452
		Schneider	0.7842	1.8260	2.2292	2.3437	2.2343	1.8416
		Chamis	0.7842	1.8270	2.2297	2.3431	2.2330	1.8390
	P100/Epoxy	Van Fo Fy	0.7842	3.1106	3.7333	4.0091	4.0908	3.9641
		Schapery	0.7842	3.1107	3.7336	4.0099	4.0923	3.9663
		Chamberlain	0.7842	3.1191	3.7533	4.0390	4.1257	3.9968
		Schneider	0.7842	3.1144	3.7533	4.0303	4.1094	3.9751
		Chamis	0.7842	3.1206	3.7525	4.0311	4.1072	3.9663
100	T300/Epoxy	Van Fo Fy	0.8932	1.7299	2.0650	2.1579	2.0730	1.7525
		Schapery	0.8932	1.7299	2.0649	2.1576	2.0725	1.7518
		Chamberlain	0.8932	1.7315	2.0687	2.1632	2.0789	1.7577
		Schneider	0.8932	1.7307	2.0677	2.1617	2.0761	1.7542
		Chamis	0.8932	1.7317	2.0681	2.1611	2.0748	1.7518
	P100/Epoxy	Van Fo Fy	0.8932	2.7332	3.1210	3.2688	3.3257	3.3048
		Schapery	0.8932	2.7333	3.1213	3.2694	3.3268	3.3067
		Chamberlain	0.8932	2.7407	3.1378	3.2931	3.3540	3.3322
		Schneider	0.8932	2.7366	3.1331	3.2860	3.3407	3.3140
		Chamis	0.8932	2.7420	3.1371	3.2867	3.3390	3.3067

Table 10. Variation of dimensionless deflections $\bar{w}$ for simply supported T300/Epoxy composite plates under sinusoidal combined loading with various fiber stacking sequences and fiber volume fractions ($\bar{T}_1 = 100$, $q_0 = 100$ and $a/h = 10$).

Fiber stacking sequence	Micromechanics-based model	V_f					
		0	0.20	0.40	0.60	0.80	1
[5°/-5°]	Van Fo Fy	0.7844	1.1009	1.1763	1.1996	1.1780	1.1027
	Schapery	0.7844	1.1009	1.1762	1.1994	1.1777	1.1022
	Chamberlain	0.7844	1.1020	1.1784	1.2025	1.1813	1.1060
	Schneider	0.7844	1.1014	1.1778	1.2017	1.1798	1.1038
	Chamis	0.7844	1.1020	1.1781	1.2014	1.1791	1.1022
[30°/-30°]	Van Fo Fy	0.7844	0.8058	0.8421	0.8574	0.8450	0.8110
	Schapery	0.7844	0.8058	0.8421	0.8572	0.8447	0.8107
	Chamberlain	0.7844	0.8065	0.8436	0.8594	0.8473	0.8134
	Schneider	0.7844	0.8061	0.8432	0.8588	0.8462	0.8119
	Chamis	0.7844	0.8066	0.8434	0.8586	0.8457	0.8107
[45°/-45°]	Van Fo Fy	0.7845	0.7413	0.7732	0.7876	0.7761	0.7470
	Schapery	0.7845	0.7413	0.7732	0.7875	0.7759	0.7466
	Chamberlain	0.7845	0.7420	0.7746	0.7895	0.7783	0.7492
	Schneider	0.7845	0.7416	0.7742	0.7890	0.7773	0.7477
	Chamis	0.7845	0.7420	0.7744	0.7888	0.7768	0.7466

Table 11. Variation of dimensionless deflections $\bar{w}_{Th}$ for simply supported T300/Epoxy composite plates under sinusoidal thermal loading with various fiber stacking sequences and fiber volume fractions ($\bar{T}_1 = 100$ and $a/h = 10$).

Fiber stacking sequence	Micromechanics-based model	V_f					
		0	0.20	0.40	0.60	0.80	1
[5°/-5°]	Van Fo Fy	0.9731	0.1806	0.1006	0.0753	0.0730	0.0930
	Schapery	0.9731	0.1802	0.1004	0.0753	0.0741	0.1015
	Chamberlain	0.9731	0.2035	0.1139	0.0756	0.0019	0.2578
	Schneider	0.9731	0.1888	0.1085	0.0754	0.0613	0.0471
	Chamis	0.9731	0.2065	0.1105	0.0754	0.0678	0.1015
[30°/-30°]	Van Fo Fy	0.9734	0.2102	0.1640	0.1506	0.1502	0.1640
	Schapery	0.9734	0.2100	0.1639	0.1506	0.1508	0.1686
	Chamberlain	0.9734	0.2227	0.1707	0.1508	0.1142	0.2535
	Schneider	0.9734	0.2147	0.1680	0.1507	0.1443	0.1390
	Chamis	0.9734	0.2243	0.1690	0.1507	0.1476	0.1686
[45°/-45°]	Van Fo Fy	0.9735	0.2813	0.2497	0.2411	0.2415	0.2526
	Schapery	0.9735	0.2811	0.2496	0.2411	0.2418	0.2556
	Chamberlain	0.9735	0.2894	0.2539	0.2412	0.2190	0.3108
	Schneider	0.9735	0.2842	0.2521	0.2411	0.2378	0.2364
	Chamis	0.9735	0.2904	0.2528	0.2411	0.2399	0.2556

Next, the impact of various parameters on the variation of normal thermal stress $\bar{\sigma}_y$ through the thickness is illustrated in Fig. 5 for T300/Epoxy laminated composite plates subjected to thermal sinusoidal loading. The variation of normal stress $\bar{\sigma}_y$ is given for various fiber volume fractions and thermal micromechanics-based models to derive the effective CTE that was previously presented and both [0°/90°] and [45°/-45°] stacking sequences are considered. It is noted that all the applied micromechanics-based models yield a similar variation in normal stress. The stacking sequence plays a crucial role in avoiding the interlaminar stress concentration that is highlighted in the [0°/90°] case. In contrast to the previous orientation system, laminate composite plates with a [45°/-45°] stacking sequence provide a continuous variation in normal stress through the thicknesses coordinate. The conclusion drawn is that interlaminar stress concentration can also arise from thermal loading, which generates the thermal stress, and can be avoided by an appropriate stacking sequence. The thermal micromechanics-based models have no major effect on the variation of normal stress through the thickness. Fig. 6 emphasizes the impact of thickness stretching in laminated composite plates exposed to thermal loading by displaying the variation of the normal out-of-plane stress $\bar{\sigma}_z$ for both [0°/90°] and [45°/-45°] laminated plates. By using the above-mentioned micromechanics-based models to predict the effective CTE, the interlaminar normal out-of-plane stress continuity is not guaranteed for the [0°/90°] stacking sequence. The presence of thermal stress $\bar{\sigma}_z$ evolves introduces discontinuities in the distribution of stress. These discontinuities have the potential to cause significant stress concentrations at the interface between the two layers. Although our model only accounts for a two-layer design, it is important to highlight that in laminates with more layers, these concentrated regions of stress at the interfaces could potentially lead to the development of delamination. Furthermore, the variation of dimensionless normal out-of-plane stress obtained by using micromechanics-based models is very close, except for the Chamberlain model, which generates a lower variation as the fiber volume fraction is increased, because it precisely uses fiber packaging geometry to determine effective transverse CTE. In contrast, the [45°/-45°] stacking sequence for laminated composite plates shows a trend opposite to the [0°/90°] sequence. The dimensionless thermal stresses $\bar{\sigma}_z$ change smoothly through the thickness, from positive out-of-plane tensile at the bottom ply to negative tensile at the top ply. Thick laminated plates require special consideration due to the significant role performed by the thermal stretching effect. The effect of fiber volume fraction and the use of the micromechanics-based model to derive the CTE on the dimensionless transverse thermal stress $\bar{\tau}_{xz}$ across the thickness are illustrated in Fig. 7. The overall thermal behavior of laminated composite plates can be significantly influenced by the transverse shear stress variation across the thickness. It is also clear that the effect of stacking sequence has an important impact on the thermal behavior of laminates. As fiber volume fraction increases, laminated plate behavior depends on the balance between fiber and matrix properties. Since the matrix has a positive CTE and the fibers have a negative CTE, as the fiber volume fraction increases, the composite's overall expansion perpendicular to the fibers may decrease. According to the particular fiber volume fraction and the embedded characteristics of the materials, it is potential that this issue might lead the composite to shrink. The observed phenomenon can be attributed to the matrix having a positive CTE, whereas the fibers demonstrate a negative CTE. As a result, this gives rise to tensile stresses in the fibers and compressive stresses in the matrix.
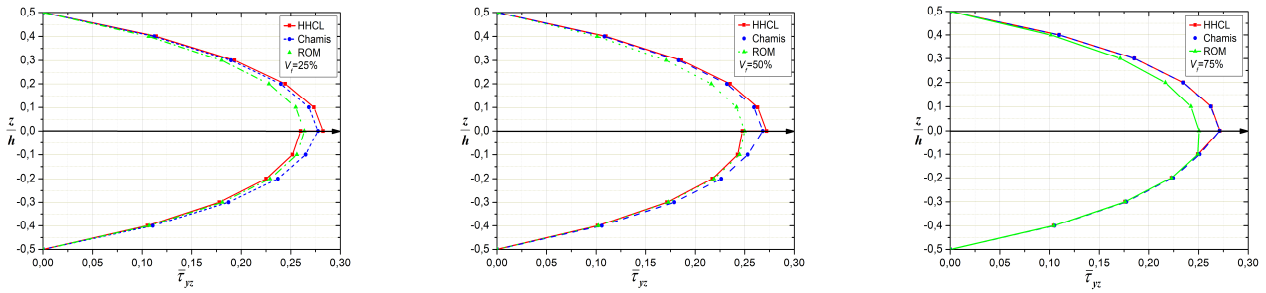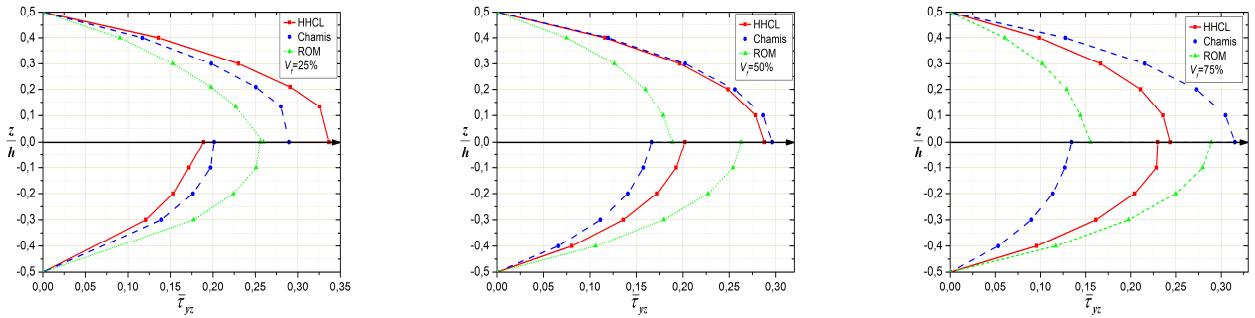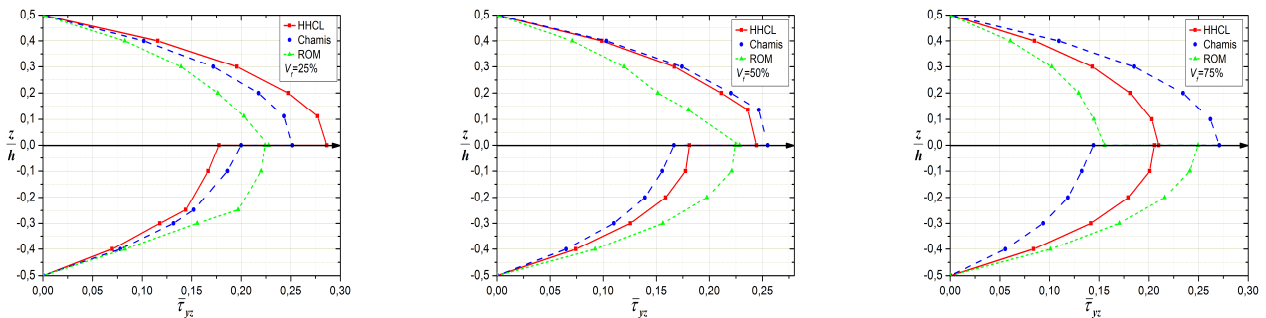
Fig. 2. Variation of dimensionless mechanical transverse stress $\bar{\tau}_{yz}$ trough the thickness coordinate for T300/Epoxy laminated composite plates [0°/90°] with various fiber volume fractions, and micromechanics-based models (*a/h=10*).
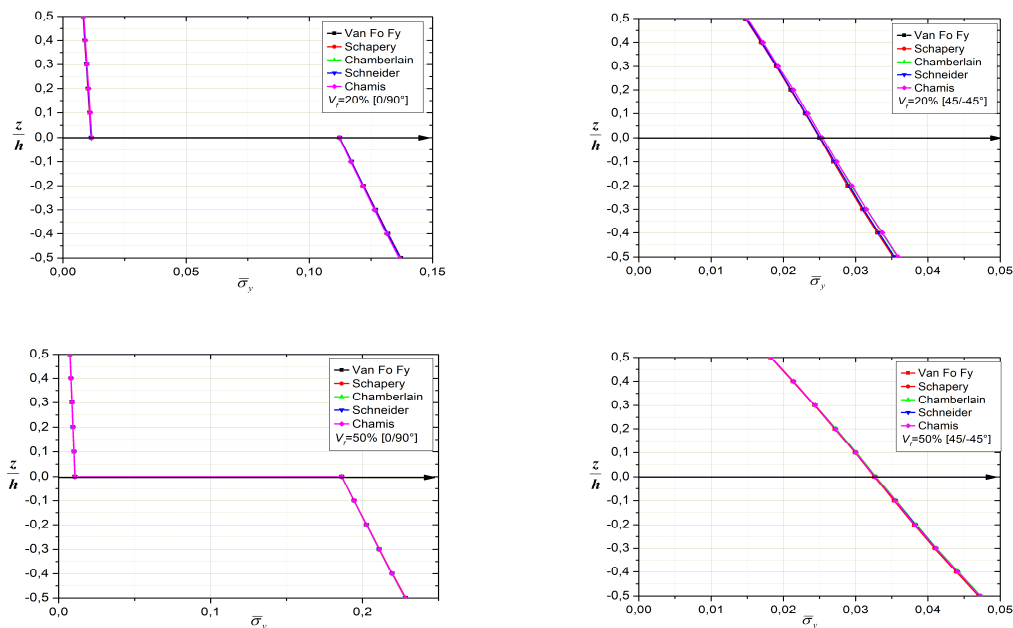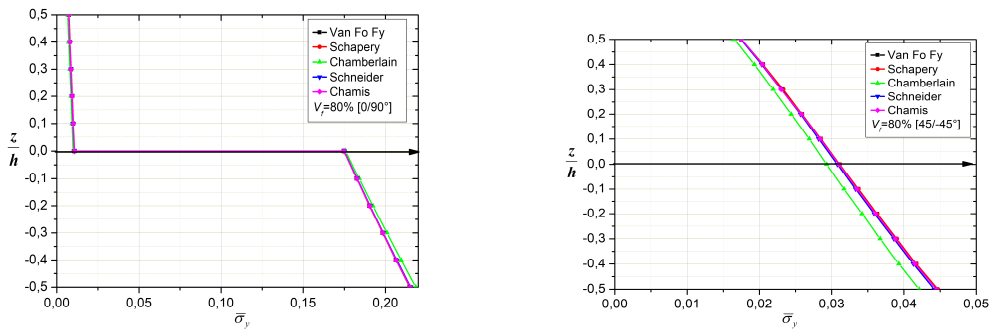

Fig. 3. Variation of dimensionless mechanical transverse stress $\bar{\tau}_{yz}$ through the thickness coordinate for HMS/Epoxy laminated composite plates [0°/90°] with various fiber volume fractions, and micromechanics-based models (*a/h=10*).

Fig. 4. Variation of dimensionless mechanical transverse stress $\bar{\tau}_{yz}$ through the thickness coordinate for P100/Epoxy laminated composite plates [0°/90°] with various fiber volume fractions and micromechanics-based models (*a/h=10*).
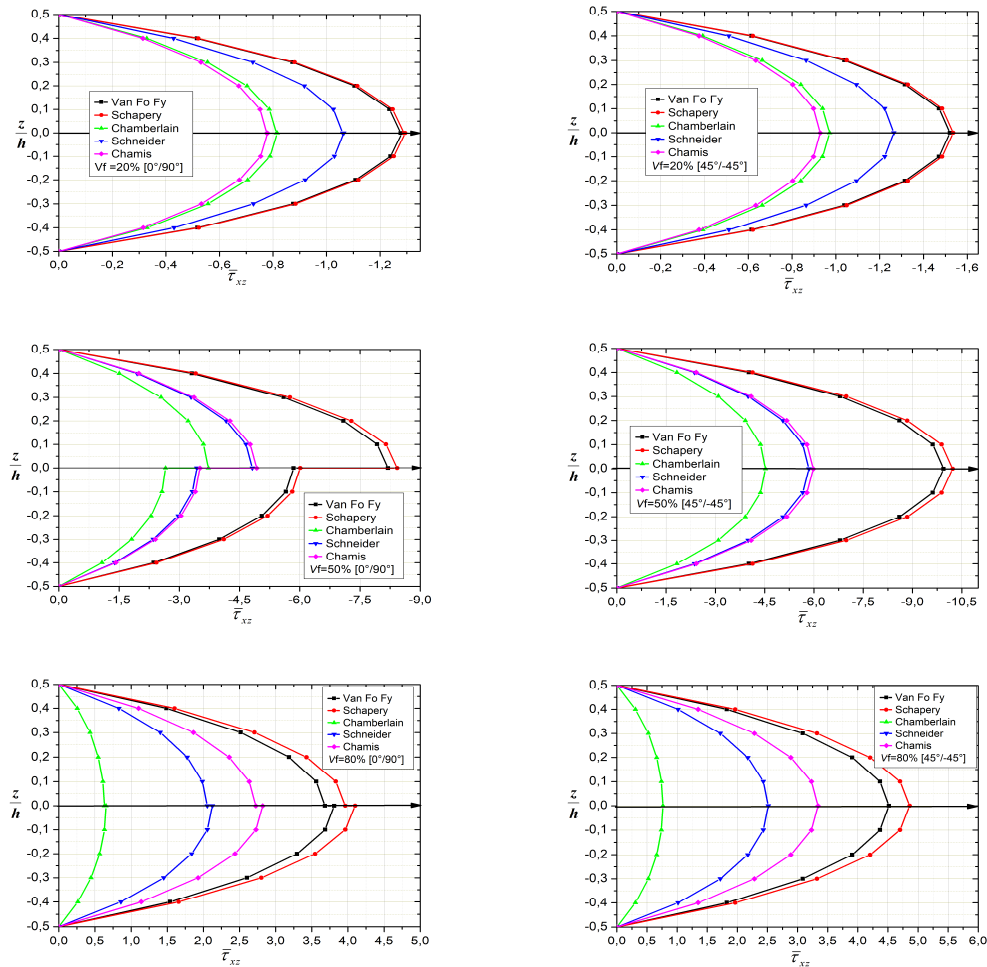

Fig. 5. Variation of dimensionless in-plane thermal stress $\bar{\sigma}_y$ through the thickness coordinate for T300/Epoxy laminated composite plates with various fiber volume fractions, fiber stacking sequences, and micromechanics-based models (*a/h=10*).

Fig. 5. Continued.
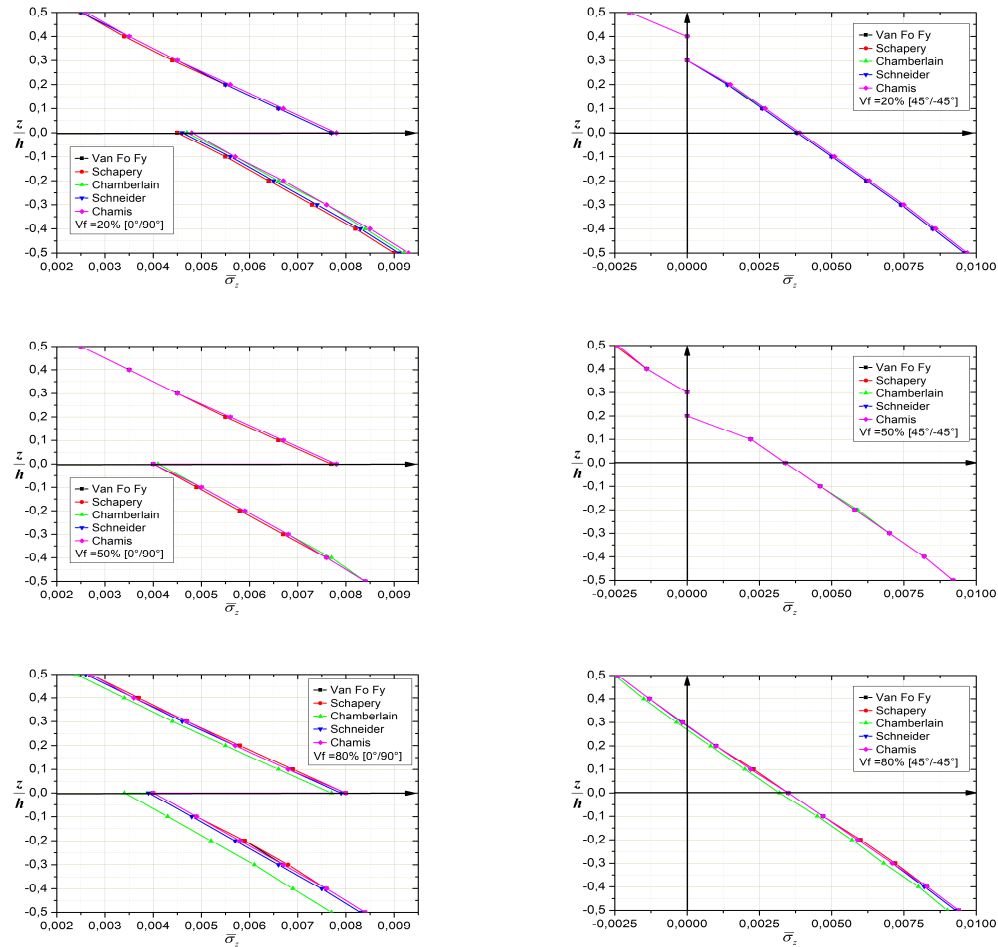
Fig. 6. Variation of dimensionless out-of-plane thermal stress $\overline{\sigma}_z$ trough the thickness coordinate for T300/Epoxy laminated composite plates with various fiber volume fractions, fiber stacking sequences, and micromechanics-based models (a/h=10).

When the fiber volume fraction is reduced, it tends to expand in the direction perpendicular to the fibers, causing compressive stresses in the fibers and tensile stresses in the matrix. This explains the positive and negative magnitudes of the dimensionless transverse thermal stress $\overline{\tau}_{xz}$ for high and low fiber volume fractions, respectively. However, it is observed that the Schapery micromechanics-based model generates a high magnitude, and the minimum magnitude is generated by the Chamberlain model, except for the reduced volume fraction, the minimum of the dimensionless transverse thermal stress is also observed in the Chamis model. As expected, the [45°/-45°] laminated plates present a smooth and continuous transition of transverse thermal stress at the interfaces of plies. According to the [0°/90°] stacking sequence, the clear difference in thermal transverse stress between the lower and upper plies can cause the occurrence of interlaminar shear stresses, which can contribute to delamination. The sensitivity of interlaminar shear stress is associated with both the stacking sequence and fiber volume fraction, as well as differences in CTE of the used composite.

In addition, it becomes evident that composite laminated plates exhibit various levels of expansion or shrinking because of the distinctive CTE exhibited by their layers. The variation in behavior between distinct layers can result in the development of stresses and strains between the layers, which could eventually contribute to the delamination and the occurrence of associated problems. This statement emphasizes the significance of employing a complete micromechanics-based model in the determination of CTE for laminated plates at the macro scale, particularly in situations involving combined mechanical and thermal loadings.

Fig. 7. Variation of dimensionless transverse thermal stress $\bar{\tau}_{xz}$ through the thickness coordinate for T300/Epoxy laminated composite plates with various fiber volume fractions, fiber stacking sequences, and micromechanics-based models ($a/h=10$).

5. Conclusions

This paper introduced a novel and efficient Quasi-3D higher-order shear and normal deformation theory for assessing the thermo-mechanical stress of laminated composite plates. The theory minimized the number of variables while investigating the thermo-mechanical responses of thick laminated composite plates. The significance of combining theory with practical discoveries was acknowledged. However, there was a lack of comprehensive research providing the specific geometric and material information necessary for direct comparison in this context. Although the inclusion of empirical data would enhance the current research, difficulties in acquiring such data have prompted us to concentrate on a comprehensive theoretical approach. This study established a strong basis for forthcoming empirical investigations and is receptive to future partnerships involving practical data. The study also investigates the assessment of alternative micromechanics-based models in predicting CTE of laminated composites, providing insights into the impact of different coefficients of thermal expansion on the obtained deflection and stresses.

The present results have revealed the emergence of several useful conclusions:

- The present theory is more accurate than other shear deformation laminated plate theories due to its thickness stretching effect.
- The longitudinal CTE of the matrix material can affect the volume fraction and stacking sequence of the fibers, leading to transverse CTE, which can cause delamination or cracks in laminated composite plates.
- Using random and arbitrary thermo-mechanical properties can lead to inaccurate results.
- Micromechanics-based schemes are essential for accurate thermo-mechanical properties.
- Micromechanics-based models can predict effective CTE, but interlaminar normal out-of-plane stress continuity is not guaranteed. Thick laminate plates require special consideration due to the thermal stretching effect.
- Schapery, Chamberlain, and Chamis models assume the same longitudinal CTE, but the Chamberlain model exhibits a higher rate of resistance to deflection and presents a range of magnitudes as the fiber volume fraction is highly increased.
- Low CTE and favorable orientation can reduce thermal stresses and sensitivity to delamination and fiber buckling, but can be unfavorable in mechanical loading applications.
- Micromechanics-based models can be used to derive the CTE, and their selection can affect the magnitude of transverse thermal stress.
- The fiber reinforcement can affect the thermal expansion of a composite material due to the differential expansion and contraction of its constituent materials.
- The mechanical loading of the laminated plate has a greater influence than the thermal loading. The Schapery model generates a higher thermal transverse stress magnitude than the other models.
- The uniform orientation of fibers provides higher stiffness and strength, resulting in a more consistent longitudinal CTE that can vary depending on the volume fraction and stacking sequence of the fibers.

- The transverse thermal stress variation across the thickness of laminated composite plates can significantly influence their thermal behavior, and this effect is affected by the fiber volume fraction and stacking sequence.

In light of the present research, it is essential to use a suitable micromechanics-based model in designing composite laminated plates, as this plays an important impact on the reliability of thermal behavior estimations. The essential roles in the current scenario are attributed to the fiber volume fraction, stacking sequence, and the overriding impact of mechanical loading over thermal loading. To enhance comprehension and application in this field, it is recommended to do further investigation into Functionally Graded Materials (FGMs), perform comprehensive experimental testing, and apply advanced numerical models within the framework of the theory's four-variable approach.

Author Contributions

N. Taibi and Z. Belabed were essential in the programming part of this project and were in charge of the preparation and presentation of the results. As the project's supervisor, Z. Belabed offered vital direction and oversight. B. Boucham, M. Benguediab, and T. Abdelouahed contributed to the conceptual framework and project proposal. K.M. Khedher and M.A. Salem carried out the review and editing procedure. All authors discussed the findings, evaluated the text, and approved the final version for publication. This author contributions section accurately depicts each author's participation in the project by indicating the precise activities that were accomplished.

Acknowledgments

Conflict of Interest

Funding

Data Availability Statements

The corresponding author can provide the datasets generated or analyzed during this study, upon a reasonable request.

Nomenclature

a, b, h	Laminated plate dimensions	k	Number of orthotropic layers
V_f, V_m	The volume fraction of fibers & matrix, respectively	k^b, k^s	The curvature of the bending and shear parts, respectively
α_1, α_2	Longitudinal and transverse CTE, respectively	m, n	Number of truncated series in the two directions of Navier solution
α_f, α_m	CTE of fibers and matrix, respectively		
E_1, E_2	Longitudinal and transverse Young modulus of composite	s, c	Sinus and Cosinus of the fiber orientation angle of the kth layer
G_{12}, G_{13}, G_{23}	Transverse shear modulus of the composite	$\nu_{23}, \nu_{13}, \nu_{12}$	Transverse Poisson's ratio of composite
E_f, E_m	Longitudinal Young modulus of fiber and matrix	ν_f, ν_m	Longitudinal–transverse Poisson's ratio of fiber and matrix
F	Packing factor for fiber (Chamberlain model)		

References

[1] Akbas, S.D., Dynamic responses of laminated beams under a moving load in thermal environment, *Steel and Composite Structures*, 35(6), 2020, 729-737.

[2] Safaei, B., The effect of embedding a porous core on the free vibration behavior of laminated composite plates, *Steel and Composite Structures*, 35(5), 2020, 659-670.

[3] Patle, B.K., Hirwani, C.K., Panda, S.K., Katariya, P.V., Dewangan, H.C., Sharma, N., Nonlinear deflection responses of layered composite structure using uncertain fuzzified elastic properties, *Steel and Composite Structures*, 35(6), 2020, 753-763.

[4] Mercan, K., Ebrahimi, F., Civalek, O., Vibration of angle-ply laminated composite circular and annular plates, *Steel and Composite Structures*, 34(1), 2020, 141-154.

[5] Al-Zahrani M.A., Asiri S.A., Ahmed K.I., Eltaher M.A., Free Vibration Analysis of 2D Functionally Graded Strip Beam using Finite Element Method, *Journal of Applied and Computational Mechanics*, 8(4), 2022, 1422-1430

[6] Mesbah, A., Belabed, Z., Tounsi, A., et al., Assessment of New Quasi-3D Finite Element Model for Free Vibration and Stability Behaviors of Thick Functionally Graded Beams, *Journal of Vibration Engineering & Technologies*, 2023, 1-17, https://doi.org/10.1007/s42417-023-00976-8.

[7] Song, Y., Hao, N., Ruan, S., He, C., Ma, Q., Free vibration properties of beetle elytron plate: Composite material, stacked structure, and boundary conditions, *Mechanics of Materials*, 185, 2023, 104754.

[8] Chan, W.S., Lin, C.Y., Liang, Y.C., Hwu, C., Equivalent thermal expansion coefficients of lumped layer in laminated composites, *Composites Science and Technology*, 66(14), 2006, 2402-2408.

[9] Fellah, M., Tounsi, A., Amara, K.H., Adda Bedia, E.A., Effect of transverse cracks on the effective thermal expansion coefficient of aged angle-ply composites laminates, *Theoretical and Applied Fracture Mechanics*, 48, 2007, 32–40.

[10] Karadeniz, Z.H., Kumlutas, D., A numerical study on the coefficients of thermal expansion of fiber reinforced composite materials, *Composite Structures*, 78(1), 2007, 1-10.

[11] Özdemir, I., Brekelmans, W.A.M., Geers, M.G.D., Computational homogenization for heat conduction in heterogeneous solids, *International Journal for Numerical Methods in Engineering*, 73, 2008, 185–204.

[12] Dong, C., Development of a model for predicting the transverse coefficients of thermal expansion of unidirectional carbon fiber reinforced composites, *Applied Composite Materials*, 15(3), 2008, 171–182.

[13] Shabana, Y.M., Noda, N., Numerical evaluation of the thermomechanical effective properties of a functionally graded material using the homogenization method, *International Journal of Solids and Structures*, 45(11–12), 2008, 3494–3506.

[14] Sakata, S., Ashida, F., Kojima, T., Stochastic homogenization analysis for thermal expansion coefficients of fiber reinforced composites using the

equivalent inclusion method with perturbation-based approach, *Computers, and Structures*, 88, 2010, 458–466.

[15] Igor, S., On the thermal expansion of composite materials and cross-property connection between thermal expansion and thermal conductivity, *Mechanics of Materials*, 45, 2011, 20–33.

[16] Nomura, S., Ball, D.L., Micromechanical formulation of effective thermal expansion coefficients of unidirectional fiber composites, *Advanced Composite Materials*, 3(2), 1993, 143-151.

[17] Tsukrov, I., Drach, B., Gross, T.S., Effective stiffness and thermal expansion coefficients of unidirectional composites with fibers surrounded by cylindrically orthotropic matrix layers, *International Journal of Engineering Science*, 58, 2012, 129–143

[18] Nawab, Y., Jaquemin, F., Casari, P., Boyard, N., Sobotka, V., Evolution of chemical and thermal curvatures in thermoset-laminated composite plates during the fabrication process, *Journal of Composite Materials*, 47, 2013, 327–339.

[19] Ran, Z.G., Yan, Y., Li, J.F., Qi, Z.X., Yang, L., Determination of thermal expansion coefficients for unidirectional fiber-reinforced composites, *Chinese Journal of Aeronautics*, 27(5), 2014, 1180–1187.

[20] Zamri, M.H., Akil, H.M., Safiee, S., Ishak, Z.A.M., Bakar, A.A., Predicting the coefficient of thermal expansion of Pultruded composites with a natural-fiber reinforcement, *Mechanics of Composite Materials*, 50, 2014, 603-612.

[21] Dong, K., Zhang, J., Cao, M., Wang, M., Gu, B., Sun, B., A mesoscale study of thermal expansion behaviors of epoxy resin and carbon fiber/epoxy unidirectional composites based on periodic temperature and displacement boundary conditions, *Polymer Testing*, 55, 2016, 44–60.

[22] Cao, H., Xiong, D.B., Tan, Z., Fan, G., Li, Z., Guo, Q., Zhang, D., Thermal properties of in situ grown graphene reinforced copper matrix laminated composites, *Journal of Alloys and Compounds*, 771, 2019, 228-237.

[23] Liang, T., Qi, L., Ma, Z., Xiao, Z., Wang, Y., Liu, H., Zhang, J., Guo, Z., Liu, C., Xie, W., Ding, T., Lu, N., Experimental study on thermal expansion coefficient of composite multi-layered flaky gun propellants, *Composites Part B*, 166, 2019, 428–435.

[24] Wang, G., An efficient analytical homogenization technique for mechanical-hygrothermal responses of unidirectional composites with applications to optimization and multiscale analyses, *Chinese Journal of Aeronautics*, 32, 2019, 382–395.

[25] Vignoli, L.L., Savi, M.A., Pacheco, P.M.C.L., Kalamkarov, A.L., Comparative analysis of micromechanical models for the elastic composite laminae, *Composites Part B*, 174, 2019, 106961.

[26] Graciani, E., Justo, J., Zumaquero, P.L., Determination of in-plane and through-the-thickness coefficients of thermal expansion in composite angle brackets using digital image correlation, *Composite Structures*, 238, 2020, 111939.

[27] Rao, Y.N., He, Q., Dai, H.L., A micromechanical model for effective hygro-thermo-elastic properties of fiber reinforced composites with functionally graded interphases, *Applied Mathematical Modelling*, 92, 2021, 78-98.

[28] Sun, Z., Shan, Z.D., Shao, T.M., Li, J.H., Wu, X.H., A multiscale modeling for predicting the thermal expansion behaviors of 3D C/SiC composites considering porosity and fiber volume fraction, *Ceramics International*, 47, 2021, 7925–7936.

[29] Zenkour, A.M., Analytical solution for bending of cross-ply laminated plates under thermomechanical loading, *Composite Structures*, 65(3-4), 2004, 367-379.

[30] Khandelwal, R.P., Chakrabarti, A., Bhargava, P., Efficient 2D thermo-mechanical analysis of composites and sandwich laminates, *Mechanics of Advanced Materials and Structures,* 26(6), 2019, 526-538.

[31] Sayyad, A.S., Ghugal, Y.M., Mhaske, B.A., A four-variable plate theory for thermoelastic bending analysis of laminated composite plates, *Journal of Thermal Stresses*, 38(8), 2015, 904-925.

[32] Ghugal, Y.M., Kulkarni, S.K., Flexural analysis of cross-ply laminated plates subjected to nonlinear thermal and mechanical loadings, *Acta Mechanica*, 224, 2013, 675-690.

[33] Qilin, J., Zhen, W., Finite element analysis of thermal stresses for laminated composites in terms of a new C⁰-type Reddy's theory, *Mechanics of Advanced Materials and Structures*, 23(6), 2016, 607-614.

[34] Naik, N.S., Sayyad, A.S., An accurate computational model for thermal analysis of laminated composite and sandwich plates, *Journal of Thermal Stresses*, 42, 2019, 559-579.

[35] Zhen, W., Xiaohui, R., Thermomechanical analysis of multilayered plates in terms of Reddy-type higher-order theory, *Mechanics of Advanced Materials and Structures*, 24(14), 2016, 1196-1205.

[36] Garg, N., Karkhanis, R.S., Sahoo, R., Maiti, P.R., Singh, B.N., Trigonometric zigzag theory for static analysis of laminated composite and sandwich plates under hygro-thermo-mechanical loading, *Composite Structures*, 209, 2019, 460-471.

[37] Joshan, Y.S., Grover, N., Singh, B.N., Analytical modelling for thermo-mechanical analysis of cross-ply and angle-ply laminated composite plates, *Aerospace Science and Technology*, 70, 2017, 137-151.

[38] Joshan, Y.S., Grover, N., Singh, B.N., New non-polynomial four variable shear deformation theory in axiomatic formulation for hygro-thermo-mechanical analysis of laminated composite plates, *Composite Structures*, 182, 2017, 685-693.

[39] Moradi, S., Mansouri, M.H., Thermal buckling analysis of shear deformable laminated orthotopic plates by differential quadrature, *Steel and Composite Structures*, 12(2), 2012, 129-147.

[40] Zenkour, A.M., Alam, M.N.M., Radwan, A.F., Bending of cross-ply laminated plates resting on elastic foundations under thermo-mechanical loading, *International Journal of Mechanics and Materials in Design*, 9(3), 2013, 239-251.

[41] Singh, S., Singh, J., Shukla, K.K., Buckling of laminated composite plates subjected to mechanical and thermal loads using meshless collocations, *Journal of Mechanical Science and Technology*, 27(2), 2013, 327-336.

[42] Liu, B., Lu, S., Ji, J., Ferreira, A.J.M., Liu, C., Xing, Y., Three-dimensional thermo-mechanical solutions of cross-ply laminated plates and shells by a differential quadrature hierarchical finite element method, *Composite Structures*, 208, 2019, 711–724.

[43] Han, J.-W., Kim, J.-S., Cho, M., Generalization of the C⁰-Type Zigzag Theory for Accurate Thermomechanical Analysis of Laminated Composites, *Composites Part B*, 122, 2017, 173-191.

[44] Zhen, W., Chen, W., A global-local higher order theory including interlaminar stress continuity and C⁰ plate bending element for cross-ply laminated composite plates, *Computational Mechanics*, 45(5), 2010, 387-400.

[45] Zuo, H., Chen, Y., Jia, F., Thermo-mechanical coupling analysis of laminated composite plates using wavelet finite element method, *Thin-Walled Structures*, 172, 2022, 108911.

[46] Upadhyay, A.K., Pandey, R., Shukla, K.K., Nonlinear flexural response of laminated composite plates under hygro-thermo-mechanical loading, *Communications in Nonlinear Science and Numerical Simulation*, 15(9), 2010, 2634-2650.

[47] Mechab, B., Mechab, I., Benaissa, S., Analysis of thick orthotropic laminated composite plates based on higher order shear deformation theory by the new function under thermo-mechanical loading, *Composites Part B*, 43(3), 2012, 1453-1458.

[48] Belbachir, N., Draich, K., Bousahla, A.A., Bourada, M., Tounsi, A., Mohammadimehr, M., Bending analysis of antisymmetric cross-ply laminated plates under nonlinear thermal and mechanical loadings, *Steel and Composite Structures*, 33(1), 2019, 81-92.

[49] Joshan, Y.S., Grover, N., Singh, B.N., Assessment of non-polynomial shear deformation theories for thermomechanical analysis of laminated composite plates, *Steel and Composite Structures*, 27(6), 2018, 761-775.

[50] Chattibi, F., Benrahou, K.H., Benachour, A., Nedri, K., Tounsi, A., Thermomechanical effects on the bending of antisymmetric cross-ply composite plates using a four variable sinusoidal theory, *Steel and Composite Structures*, 19(1), 2015, 93-110.

[51] Ameri, A., Fekrar, A., Bourada, F., Selim, M.M., Benrahou, K.H., Tounsi, A., Hussain, M., Hygro-thermo-mechanical bending of laminated composite plates using an innovative computational four variable refined quasi-3D HSDT model, *Steel and Composite Structures*, 41(1), 2021, 31-44.

[52] Maji, A., Mahato, P.K., Development, and applications of shear deformation theories for laminated composite plates: an overview, *Journal of Thermoplastic Composite Materials*, 35(12), 2020, 2576-2619.

[53] Mahapatra, T.R., Panda, S.K., Kar, V.R., Nonlinear flexural analysis of laminated composite panel under hygrothermo-mechanical loading - A micromechanical approach, *International Journal of Computational Methods*, 13(3), 2016, 1650015.

[54] Saidane, E.H., Scida, D., Ayad, R., Thermo-mechanical behaviour of flax/green epoxy composites: Evaluation of thermal expansion coefficients and application to internal stress calculation, *Industrial Crops and Products*, 170, 2021, 113786.

[55] Reddy, J.N., *Mechanics of Laminated Composite Plates and Shells: Theory and Analysis*, 2nd ed., CRC Press, 2004.

[56] Mehala, T., Belabed, Z., Tounsi, A., Beg, O.A., Investigation of influence of homogenization models on stability and dynamic of FGM plates on elastic foundations, *Geomechanics and Engineering*, 16(3), 2018, 257-271.

[57] Van Fo Fy, G.A., Basic relations of the theory of oriented glass-reinforced plastics (GRP) with hollow fibers, *Polymer Mechanics*, 2, 1966, 478–483.

[58] Schapery, R.A., Thermal expansion coefficients of composite materials based on energy principles, *Journal of Composite Materials*, 2(3), 1968, 380-

404.

[59] Sideridis, E., Thermal expansion coefficients of fiber composites defined by the concept of the interphase, *Composites Science and Technology*, 51(3), 1994, 301-317.

[60] Rogers, K.F., Phillips, L.N., Kingston-Lee, D.M., Yates, B., Overy, M.J., Sargent, J.P., McCalla, B.A., The thermal expansion of carbon fibre-reinforced plastics: Part 1 The influence of fiber type and orientation, *Journal of Materials Science*, 12, 1977, 718-734.

[61] Huang, Z.M., Simulation of the mechanical properties of fibrous composites by the bridging micromechanics model, *Composites Part A*, 32(2), 2001, 143-172.

[62] Hong, Y., Yan, Y., Guo, F., Li, X., Tian, Z., Predicting the elastic properties of 3D N-directional braided composites via a theoretical method, *Mechanics of Composite Materials*, 55, 2019, 95-106.

[63] Hopkins, D.A., Chamis, C.C., A unique set of micromechanics equations for high temperature metal matrix composites, *Composite Materials: Testing and Design*, 964, 1988, 159-176.

[64] Christensen, R., Lo, K., Solutions for effective shear properties in three phase sphere and cylinder models, *Journal of the Mechanics and Physics of Solids*, 27(4), 1979, 315-330.

[65] Belabed, Z., Selim, M.M., Slimani, O., Taibi, N., Tounsi, A., Hussain, M., An efficient higher order shear deformation theory for free vibration analysis of functionally graded shells, *Steel and Composite Structures*, 40, 2021, 307-321.

[66] Mesbah, A., Belabed, Z., Amara, K., Tounsi, A., Bousahla, A.A., Bourada, F., Formulation, and evaluation a finite element model for free vibration and buckling behaviours of functionally graded porous (FGP) beams, *Structural Engineering and Mechanics*, 86(3), 2023, 291–309.

[67] Reddy, J.N., Hsu, Y.S., Effects of shear deformation and anisotropy on the thermal bending of layered composite plates, *Journal of Thermal Stresses*, 3(4), 1980, 475493.

[68] Pagano, N.J., Exact solutions for rectangular bidirectional composites and sandwich plates, *Journal of Composite Materials*, 4(1), 1970, 20-34.

[69] Reddy, J.N., A simple higher order theory for laminated composite plates, *Journal of Applied Mechanics*, 51(4), 1984, 745-752.

[70] Mindlin, R.D., Influence of rotary inertia and shear on flexural motions of isotropic elastic plates, *Journal of Applied Mechanics*, 18, 1951, 31-38.

[71] Kim, S.E., Thai, H.T., Lee, J., A two variable refined plate theory for laminated composite plates, *Composite Structures*, 89, 2009, 197-205.

ORCID iD

Noureddine Taibi https://orcid.org/0009-0001-3041-6184
Zakaria Belabed https://orcid.org/0000-0003-4756-7971
Belhadj Boucham https://orcid.org/0009-0002-0440-7142
Mohamed Benguediab https://orcid.org/0000-0002-6595-5786
Abdelouahed Tounsi https://orcid.org/0000-0002-5601-3228
Khaled Mohamed Khedher https://orcid.org/0000-0002-4167-1690
Mohamed Abdelaziz Salem https://orcid.org/0000-0002-9344-0931

Publisher's Note Shahid Chamran University of Ahvaz remains neutral with regard to jurisdictional claims in published maps and institutional affiliations.